Published in final edited form as:
Stem Cells. 2010 August ; 28(8): 1355–1367. doi:10.1002/stem.465.

ATP-Sensitive K+ Channel-Deficient Dilated Cardiomyopathy Proteome Remodeled by Embryonic Stem Cell Therapy

Jelena Zlatkovic-Lindor, **D. Kent Arrell**, **Satsuki Yamada**, **Timothy J. Nelson**, and **Andre Terzic**
Marriott Heart Disease Research Program, Division of Cardiovascular Diseases, Departments of Medicine, Molecular Pharmacology and Experimental Therapeutics, and Medical Genetics, Mayo Clinic, Rochester, Minnesota, USA

Abstract

Transplantation of pluripotent stem cells has proven beneficial in heart failure, yet the proteomic landscape underlying repair remains largely uncharacterized. In a genetic model of dilated cardiomyopathy elicited by pressure overload in the *KCNJ11* (potassium inwardly rectifying channel, subfamily J, member 11) null mutant, proteome-wide profiles were here resolved by means of a systems approach prior to and following disease manifestation in the absence or presence of embryonic stem cell treatment. Comparative two-dimensional gel electrophoresis revealed a unique cardiomyopathic proteome in the absence of therapy, remodeled in response to stem cell treatment. Specifically, linear ion trap quadrupole-Orbitrap mass spectrometry determined the identities of 93 and 109 differentially expressed proteins from treated and untreated cardiomyopathic hearts, respectively. Mapped protein– protein relationships and corresponding neighborhoods incorporated the stem cell-dependent subproteome into a nonstochastic network with divergent composition from the stem cell-independent counterpart. Stem cell intervention produced a distinct proteome signature across a spectrum of biological processes ranging from energetic metabolism, oxidoreductases, and stress-related chaper-ones to processes supporting protein synthesis/degradation, signaling, and transport regulation, cell structure and scaffolding. In the absence of treatment, bioinformatic interrogation of the disease-only proteome network prioritized adverse cardiac outcomes, ablated or ameliorated following stem cell transplantation. Functional and structural measurements validated improved myocardial contractile performance, reduced ventricular size and decreased cardiac damage in the treated cohort. Unbiased systems assessment unmasked “cardiovascular development” as a prioritized biological function in stem cell-reconstructed cardiomyopathic hearts. Thus, embryonic stem cell treatment transformed the cardiomyopathic proteome to demote disease-associated adverse effects and sustain a procardiogenic developmental response, supplying a regenerative substrate for heart failure repair.

Correspondence: Andre Terzic, M.D., Ph.D., Mayo Clinic, Stabile 5, 200 First Street SW, Rochester, Minnesota 55905, USA. Telephone: +1-507-284-2747; Fax: +1-507-266-9936; terzic.andre@mayo.edu.

Author contributions: J.Z.L.: conception and design, collection and/or assembly of data, data analysis and interpretation, manuscript writing, final approval of manuscript; D.K.A.: conception and design, collection and/or assembly of data, data analysis and interpretation, manuscript writing, final approval of manuscript; S.Y.: conception and design, provision of study material, collection and/ or assembly of data, data analysis and interpretation, manuscript writing, final approval of manuscript; T.J.N.: conception and design, provision of study material, data analysis and interpretation, manuscript writing, final approval of manuscript; A.T.: conception and design, financial support, administrative support, data analysis and interpretation, manuscript writing, final approval of manuscript.

Disclosure of Potential Conflicts of Interest.
The authors indicate no potential conflicts of interest.

Keywords

ATP-sensitive K^+ channel; Bioinformatics; K_{ATP} channel; Dilated cardiomyopathy; Protein expression; Genetics; Networks; Proteomics; Regenerative medicine

INTRODUCTION

Cardiomyopathy is an intrinsic, progressive disorder of the myocardium resulting in impaired function of the heart [1]. The clinical entity of dilated cardiomyopathy is characterized by ventricular dilation and reduced contractile performance, precipitating heart failure and poor outcome [2, 3]. Discovery of monogenic forms of heritable dilated cardiomyopathy has revealed the intricate nature of corrupted pathways independent of common risk factors such as ischemic disease, underlying endocrine disorders or cardiotoxic insults [4–7]. A case in point is the recent genetic studies linking defects in cardioprotective ATP-sensitive K^+ (K_{ATP}) channels to an aberrant stress response in the pathogenesis of a malignant form of dilated cardiomyopathy [8–12]. Severity of disease progression in dilated cardiomyopathy often mandates cardiac transplantation as the only remaining treatment option, a constraint compounded by donor organ shortage, warranting exploration of alternative management strategies [12, 13].

Beyond the reach of current therapies, stem cell technology provides a foundation for heart repair without the need for organ replacement [14–18]. Although cardiac rejuvenation has been recognized as a homeostatic self-repair mechanism, the innate regenerative reserve is insufficient to salvage failing myocardium [19–22]. In fact, initiation and evolution of the cardiomyopathic process was linked to depletion of the resident cardiac stem cell pool [23]. Introduction of progenitor cells into the diseased heart may therefore offer a means of promoting the healing process. Indeed, in the context of K_{ATP} channel ablation that recapitulates salient traits of the human dilated cardiomyopathy 1O syndrome (CMD 1O), functional repair was recently achieved by an embryonic stem (ES) cell therapy regimen [24]. Moreover, it has been established that embryonic stem cell progeny consistently acquire a cardiogenic phenotype with functional excitation-contraction coupling associated with maturation of the cellular energetic matrix, and when transplanted into damaged heart contribute to repopulation of dysfunctional myocardium improving contractile performance [25–29]. Stem cell lineage commitment and integration within diseased host myocardium has been further documented [30– 33]. Deciphering the molecular substrate underlying the regenerative process would however require mapping the protein landscape of the recipient heart in response to stem cell intervention. So far, however, the proteomic response of cell therapy in heart disease remains unknown.

Enabled by high-throughput technologies for large scale identification of proteins and associated networks, systems platforms offer an integrative, unbiased approach to address the complexity of pathobiologic change in disease and in response to therapy [34–38]. Here, in the stressed K_{ATP} channel knockout, a prototype of genetic dilated cardiomyopathy, proteome-wide profiling decoded the global manifestation of disease and the signature of embryonic stem cell therapy. In the stem cell-dependent proteome, network analysis demonstrated a prioritized cardiovascular development function and demotion of disease-associated adverse effects, validated by improved functional and structural outcome with treatment. Stem cell-based proteomic remodeling is thus resolved in a genetic model of dilated cardiomyopathy, mapping molecular underpinnings of regenerative outcome.

MATERIALS AND METHODS

Genetic Model of Dilated Cardiomyopathy and Intervention Protocols

Protocols were carried out in accordance with NIH guidelines, and with approval of the Institutional Animal Care and Use Committee. Eight- to twelve-week-old male K_{ATP} channel knockout mice (Kir6.2-KO), generated by disruption of the *KCNJ11* (potassium inwardly rectifying channel, subfamily J, member 11) gene encoding the Kir6.2 channel pore [9, 24], served as the prestress Control cohort (experimental group 1). Separate cohorts of syngeneic age- and sex-matched Kir6.2-KO mice underwent transverse aortic constriction (TAC) to induce continuous hemodynamic pressure overload upon the left ventricle [39, 40]. At 2 weeks following aortic constriction, pressure-overloaded Kir6.2-KO hearts were exposed by thoracotomy, and animals were further randomly separated into two disease groups, that is, untreated [ES(−), experimental group 2] and embryonic stem cell treated [ES(+), experimental group 3]. Study subjects uniformity across cohorts ensured controlled head-to-head comparisons of experimental interventions. For the ES(+) cohort, epicardial injection of 200,000 murine lacZ-labeled R1 embryonic stem cells, in 15 μl propagation medium (Glasgow's Minimum Essential Medium, Lonza, Basel, Switzerland), was performed at five separate sites (40,000 cells in 3 μl per site) in the anterior wall of the left ventricle [24]. The R1 embryonic stem cell line was selected as it is the only cell type demonstrated to ensure repair in this model of genetic dilated cardiomyopathy [24]. End points included survival, cardiac function and structure evaluated by echocardiography and pathological examination [24], as well as proteome-wide and network analysis. Functional parameters were measured at a series of time points, including at baseline and at 1.5, 2, 4, and 8 weeks postaortic constriction, with additional comparative tracking of contractile and structural changes in ES(−) versus ES(+) cohorts at 0, 2, and 6 weeks postrandomization for cell intervention. The time point of 8 weeks was selected for proteomic analysis as indices of disease progression were consistent with chronic end-stage heart failure. Because of high mortality of K_{ATP} channel knockout animals [24, 40], a total of 90 animals were required in the study to assure sufficient survivorship up to 8 weeks of sustained stress load.

Prospective Evaluation of Cardiac Function and Structure

To evaluate progression of disease and the impact of stem cell therapy, transthoracic echocardiography (30-MHz MS400 transducer, Vevo2100, Visual Sonics, Toronto, Canada; 15L8 transducer, Sequoia 512, Siemens, Concord, CA) [41] was performed at multiple time points to prospectively assess cardiac function and structure. For all experimental groups, left ventricular fractional shortening (%) was calculated as ([LVDd – LVDs]/ LVDd) × 100, where LVDd is left ventricular end-diastolic dimension (mm) and LVDs, left ventricular end-systolic dimension (mm) [42]. Ejection fraction (%) was calculated as ([LVVd – LVVs]/LVVd) × 100, where LVVd is left ventricular end-diastolic volume (μl) and LVVs, left ventricular end-systolic volume (μl). Left ventricular weight (mg) was derived as $[(LVDd + IVST + PWT)_3 – LVDd_3] \times 1.055$, where IVST is interventricular septum thickness (mm), and PWT, posterior wall thickness (mm). Left ventricular wall thickness to dimension ratio was calculated as a sum of IVST and PWT divided by LVDd, and was used to monitor the evolution of heart geometry [24, 33, 40]. Total heart weight was measured at the time of autopsy.

Protein Extraction and Quantitation

For proteomic analysis, disease-untreated [ES(−)] and disease-treated [ES(+)] Kir6.2-KO, as well as prestress unconstricted (control) animals, were sacrificed under isoflurane anesthesia, and hearts excised and rinsed in phosphate-buffered saline. Left ventricles including septum were removed, weighed ex vivo, snap-frozen in liquid N_2, and stored at −80°C. Cytosolic tissue extracts, comprising the majority of cellular proteins compatible

with isoelectric focusing (IEF) solubilization and resolution, were prepared by homogenization at 4°C in four volumes of extraction buffer, consisting of (in mM) 4-(2-hydroxyethyl)-1-ppiperazineethanesulfonic acid (HEPES) 25 (pH 7.4), phenyl-methylsulfonyl fluoride (PMSF) 0.25, and dithiothreitol (DTT) 50, 1.25 μM pepstatin A, Mini-Complete protease inhibitor cocktail (Roche Applied Science, Indianapolis, IN), and 1% phosphatase inhibitor cocktails 1 and 2 (Sigma, St. Louis, MO) [43]. Samples were centrifuged (16,000g) at 4°C for 10 minutes, supernatants were transferred to fresh tubes, and protein was quantified in triplicate by Bio-Rad (Hercules, CA) protein assay using the microassay procedure with a bovine γ-globulin standard [44], with equivalent protein amounts from all samples resolved simultaneously by sodium dodecyl sulfate polyacrylamide gel electrophoresis (SDS-PAGE) and stained to independently assess protein quantitation prior to two-dimensional (2D) gel electrophoresis.

2D Electrophoresis and Gel Imaging

Protein extracts (100 μg) were resolved by immobilized pH gradient (IPG) 2-DE following addition to IEF rehydration buffer (7 M urea, 2 M thiourea, 2% w/v CHAPS, 50 mM DTT, 1 × Bio-Rad pH 3–10 ampholytes). Same lot IPG Ready Strips (pH 3–10, 170 mm, Bio-Rad) were actively rehydrated at 50 V for 10 hours, followed by rapid voltage ramping with a series of 15 minutes steps at 100, 500, and 1,000 V, and a final step at 10,000 V for 60 kVh at 20°C [45]. Focused IPG strips were rinsed with distilled, deionized water, and incubated for 15 minutes in equilibration buffer (50 mM Tris-HCl, pH 8.8, 6 M urea, 30% v/v glycerol, 2% w/v SDS) containing 10 mg/ml DTT, followed by 15 minutes in equilibration buffer containing 25 mg/ml iodoacetamide. After horizontal positioning on freshly prepared 12.5% SDS-PAGE gels, strips were overlaid with SDS buffer (25 mM Tris, 192 mM glycine, 0.1% w/v SDS) containing 0.5% w/v agarose, and resolved orthogonally by SDS-PAGE in a Protean II XL system (Bio-Rad). Resolved 2D gels were silver stained and digitized at 400 dpi for spot image analysis, including spot detection, matching, normalization, and quantification, conducted with Bio-Rad PDQuest v.7.4.0 following subtraction of background and horizontal/vertical streaking intensities [36, 43]. Individual gel images were normalized by total intensity of valid spots. Fold change ratios were calculated as [mean ES(−)]:[mean Control], [mean ES(+)]:[mean Control], and [mean ES(+)]:[mean ES(−)] for protein spots increasing in the numerator group, or the negative inverse for protein species decreasing in the numerator group. For proteins identified in more than one spot, the sum of values for all spots was used to determine a weighted average treatment ratio, unless otherwise indicated.

Nanoelectrospray Linear Ion Trap Tandem Mass Spectrometry

Significantly altered protein species were isolated from resolved gels, destained, and prepared for liquid chromatography-tandem mass spectrometry (LC-MS/MS) by reduction, alkylation, tryptic digestion, peptide extraction, and drying [32, 38, 43]. Peptides were reconstituted in 0.15% formic acid, 0.05% trifluoroacetic acid (TFA), and trap injected onto a 75 μm × 10 cm ProteoPep C18 PicoFrit nanoflow column (New Objective, Woburn, MA). Chromatography was performed using 0.2% formic acid in solvent A (99% water, 1% acetonitrile) and B (80% acetonitrile, 5% isopropanol, 15% water), with peptides eluted over 30 minutes with a 5%–45% solvent B gradient using an Eksigent nanoHPLC system (MDS Sciex, Toronto, Canada) coupled to a linear ion trap quadrupole (LTQ)-Orbitrap mass spectrometer (Thermo Fisher Scientific, Barrington, IL). Continuous scanning of eluted peptide ions was carried out between 375 and 1600 *m/z*, automatically switching to MS/MS collision induced dissociation mode on ions exceeding an intensity of 8,000. Raw MS/MS spectra were converted to .dta files using Bioworks 3.2 (Thermo Fisher Scientific), and merged files matching +1, 2, or three peptide charge states were correlated to theoretical tryptic fragments in Swiss-Prot (v.53.0) using Mascot v.2.2 [46]. Searches were conducted

on mammalian sequences (53,539 entries), tolerating up to two missed cleavages, a mass tolerance of 60.01 Da for precursor ions (including ^{13}C peak detection) and 60.6 Da for MS/MS product ions allowing for protein N-terminal acetylation, methionine oxidation, and cysteine carbamidomethylation. Protein identities were confirmed by matching multiple peptide spectra at $p < .05$, with proteins accepted at $p < .01$. Proteins identified by a single peptide were thus subjected to a higher stringency level ($p < .01$), and were confirmed by manual spectrum inspection with detected fragment ions from the MS/MS spectrum required to be above baseline noise, have demonstrable continuity in b-or y-ion series, and proline residues yielding intense y-ions [47]. Protein assignments were further validated by congruence of observed versus predicted pI/M_r, using the ExPASy pI/M_r tool (http://us.expasy.org/tools/pi_tool.html), taking into consideration protein processing and post-translational modifications.

Interactome Network Analysis

Differentially expressed proteins, with fold change ratios, were submitted as focus proteins for network analysis using Ingenuity Pathways Knowledge Base (Ingenuity Systems, www.ingenuity.com) to identify associated functional networks. An overview of interactions was obtained by merging functional subnetworks into composite interactomes. The composites were depicted using the molecular interaction network visualization program Cytoscape 2.6.2 [48], with paired network layouts coordinated using the ReOrientPlugin to localize common nodes in the same spatial location within multiple networks, and topological properties characterized using Network Analyzer [49]. Computed properties included node degree (k), the number of links connected to the node, and node degree distribution [P(k)], the probability that a specified node has k links, defined as $P(k) = X(k)/n$, where $X(k)$ is the number of nodes with degree k and n is the total number of network nodes [50, 51]. P(k) versus k discriminates between random and scale-free topographies, defined by normal and power law distributions, respectively [50]. The Anderson-Darling normality test ruled out a normal distribution, so P(k) versus k was calculated as a power law relationship using a cumulative distribution function [52] to determine γ in the power law distribution [$P(k) \sim k^{-\gamma}$] according to Equation (1):

$$\gamma = 1 + n\left[\sum_{i=1}^{n} \ln \frac{x_i}{x_{\min}}\right]^{-1} \quad (1)$$

where γ is the power law exponent, n the number of network nodes, x_i node degree, and $x_{\min}$ the minimum node degree within the network, with statistical error σ [52] for Equation (1) defined by Equation (2):

$$\sigma = \sqrt{n}\left[\sum_{i=1}^{n} \ln \frac{x_i}{x_{\min}}\right]^{-1} = \frac{\gamma - 1}{\sqrt{n}} \quad (2)$$

To link expression data with systems functions, resolved networks were interrogated with Ingenuity Pathways Analysis (IPA) [36, 43].

Statistical Analysis

Comparison between groups was performed using a standard t-test of variables with 95% confidence intervals, with data expressed as mean ± standard error. Wilcoxon test was used to evaluate cardiac physiological parameters (JMP 8, SAS Institute, Cary, NC). Kaplan-Meier analysis with log-rank testing was applied to evaluate survivorship. Comparison of

2D gel spot intensities between experimental groups was carried out by *t*-test. A $p < .05$ was considered significant, unless otherwise indicated.

RESULTS

Global Protein Profiling in Genetic Cardiomyopathy and Stem Cell Intervention

TAC imposes sustained pressure overload on the left ventricle resulting over 8 weeks in progressive contractile dysfunction and cardiomegaly, characteristic of congestive heart failure in the *KCNJ11* knockout, Kir6.2-KO model (Fig. 1A), a surrogate of human genetic K_{ATP} channel-deficient cardiomyopathy [24, 40]. To assess, in the setting of K_{ATP} channel deficiency, molecular consequences of TAC-imposed stress in the absence and presence of stem cell intervention, prestressed *KCNJ11* knockouts (control, experimental group 1) were compared head-to-head to pressure-overloaded Kir6.2-KO randomized at 2 weeks post-TAC into untreated [ES(−), experimental group 2] and embryonic stem cell-treated [ES(+), experimental group 3] cohorts (Fig. 1B). To this end, left ventricle cytosolic proteomes were extracted from control ($n = 5$), and 8 weeks after TAC from ES(−) ($n = 5$) and ES(+) ($n = 5$) cohorts, and profiled by differential proteomics. In broad pH range silver-stained 2D gels (Fig. 1C), over 700 protein species were consistently resolved (Fig. 1D). Reproducibility across cohorts was documented by positive correlation of average normalized intensities of matching protein spots in control versus ES(−) and control versus ES(+) gels (Fig. 1E and 1F, scatter plots). Densitometric quantification revealed that a subset of 84 unique protein spots (12% of resolved proteome) was significantly altered in response to TAC-induced pressure overload in the cardiomyopathic K_{ATP} channel knockout hearts [control vs. ES(−); Fig. 1E, pie chart]. Following 6 week-long cell therapy, 44 protein spots (7% of resolved proteome) differed between prestressed controls and stem cell-treated TAC Kir6.2-KO [control vs. ES(+); Fig. 1F, pie chart]. Thus, differential expression profiling of Kir6.2 K_{ATP} channel knockout hearts demonstrated the global proteomic impact of imposed stress, with cell therapy eliciting distinct remodeling of the cardiomyopathic subproteome in stressed failing hearts.

Distinct Protein Signatures in Cardiomyopathic Hearts in Absence and Presence of Stem Cell Therapy

Proteins specifically altered in failing K_{ATP} channel knockout hearts, in the absence and presence of stem cell therapy, were determined by LTQ-Orbitrap MS/MS analysis of in-gel tryptic digests. In ES(−) hearts, 109 altered proteins were identified by this high-throughput approach. Individual protein identities, along with extent of fold-change and supporting gel and mass spectrometry metrics, encompass a spectrum across metabolism and signaling infrastructure reflecting the complex pathologic substrate of the cardiomyopathic state (Fig. 2; Supporting Information Table S1 and Table S2). Cellular metabolism related identities were responsible for 64% of disease-induced proteome change, and included 13 oxidative phosphorylation, 13 tricarboxylic acid (TCA) cycle, and 44 substrate metabolism proteins (Fig. 2). Ontological annotation revealed that the additional 39 identified proteins formed a metabolism-related signaling infrastructure encompassing oxidoreductases (10 proteins), cellular structure and scaffolding (11), signaling regulation (3), stress-related chaperones (8), protein synthesis and degradation (3), as well as transport regulation (4) (Fig. 2). In ES(+) hearts, a distinct set of 93 proteins were identified in response to stem cell treatment (Fig. 3; Supporting Information Table S1 and Table S3). These were primarily associated with metabolism (63 proteins, 68%), including oxidative phosphorylation (8 proteins), TCA cycle (12) and substrate metabolism (43), and a metabolism-related infrastructure of oxidoreductases (10), cellular structure and scaffolding (3), signaling regulation (4), stress-related chaperones (5), protein synthesis and degradation (5), as well as transport regulation (3) (Fig. 3). When compared with untreated hearts (Fig. 2), cell therapy (Fig. 3) nullified

disease-induced changes in 68% of proteins and reduced the extent of fold-change in an additional 16%, reorganizing the proteome landscape of failing hearts. Thus, resolving individual identities of protein changes establishes a signature of K_{ATP} channel-deficient cardiomyopathy, extensively restructured by stem cell intervention.

Stem Cell Treatment Restructures Cardiomyopathic Proteome Network

To obtain a collective understanding of processes associated with cell therapy-induced proteome remodeling in the setting of K_{ATP} channel deficient cardiomyopathy, network analysis was implemented to compare untreated ES(−) versus treated ES(+) subproteomes. Protein–protein interaction mapping clustered the 109 altered proteins from untreated cardiomyopathic hearts into an organized network comprised of 229 nodes linked by 1,207 interactions [or edges; Fig. 4A, left; ES(−) network]. The 93 proteins specific to the stem cell-treated diseased hearts assembled into a network of 205 nodes connected by 975 edges [Fig. 4A right, ES(+) network]. Network topologies for both ES(−) and ES(+) networks displayed a nonstochastic pattern, excluding a random association among changing proteins. Indeed, the inter-relationship between node degree (k) and degree distribution P(k) followed power law distributions indicative of scale-free nonrandom architecture (Fig. 4A, insets left and right). Although similar in size, the two networks shared only 75 common proteins (Fig. 4B), underscoring the distinct molecular composition of the ES(−) and ES(+) proteomes expanded to a broader network neighborhood context. The majority of proteins in every functional category were unique to each of the respective networks, as only 35% of metabolic proteins and fewer than 22% of nodes for any metabolism-related infrastructure category were shared between ES(−) and ES(+) networks (Fig. 4C). Thus, mapped ES(−) and ES(+) heart subproteome-dependent networks exhibit limited overlap, suggesting different functional consequences in the absence and presence of stem cell therapy.

In Silico Phenotypic Patterns Induced by Stem Cell Therapy Validated In Vivo

Network analysis provides a systems framework to delineate, in an impartial manner, putative patterns arising from a remodeled proteome based on extracted core signatures [35, 38]. Collective bioinformatic interrogation demonstrated a dramatically overrepresented “Cardiac Disease” category associated with the ES(−) network ($p = 2.35 \times 10^{-5}$), consistent with heart disease susceptibility, which was reduced by three orders of magnitude ($p = 3.11 \times 10^{-2}$) within the ES(+) network (Fig. 5A, left). Further interrogation of the ES(−) network against a broad spectrum of 134 curated pathological conditions and toxicological pathways within the Ingenuity Pathways Knowledge Base extracted exclusively cardiac structural and functional adverse effects, namely “cardiac damage,” “cardiac dilation,” “cardiac dysplasia,” “cardiac enlargement,” “cardiac inflammation,” “cardiac hypertrophy,” and “cardiac fibrosis” (Fig. 5A, right). Bioinformatic survey predicted that the six of these seven detrimental outcomes in the ES(−) network are eliminated from the ES(+) network, suggesting functional and structural benefit of stem cell intervention in the setting of cardiomyopathy (Fig. 5A, right). To validate this core prediction, cardiac function and structure were assessed in vivo in untreated and stem cell-treated cohorts by prospective echocardiography (Fig. 5B–5G) and pathoanatomical analysis (Fig. 5H–5I). Untreated Kir6.2-KO-stressed mice [ES(−)] demonstrated significant and progressive cardiac dysfunction (Fig. 5B–5G) and associated heart chambers enlargement (Fig. 5H–5I), precipitating without therapy high mortality rates with 53% survivorship between 2 and 8 weeks poststress and poor overall survival (17%). In contrast, throughout the follow-up period, stem cell intervention [ES(+)] significantly improved cardiac contractility and prevented cardiac dilation and enlargement, nullifying premature mortality. Specifically, serial monitoring of fractional shortening from the point of randomization 2 weeks post-TAC indicated continuous deterioration without cell therapy, but improved fractional shortening with cell therapy at multiple time points (Fig. 5C). Ejection fraction, an index of

cardiac contractility that prognosticates outcome in heart failure, was reversed towards prestress levels by stem cell treatment (i.e., 22.4 ± 2.4%, $n = 5$ ES(−) vs. 69.1 ± 3.3%, $n = 5$ ES(+), $p < .01$, with control 95% confidence interval indicated for benchmarking; Fig. 5D). The post-TAC increase in cardiac dilation in untreated hearts was marked by 2 weeks and continuously increased by 6 weeks, whereas cell therapy was effective in maintaining diastolic dimension throughout the observation period (Fig. 5E). Significant wall thinning relative to left ventricular diameter without treatment was restored to control levels 6 weeks following cell delivery (i.e., 0.33 ± 0.04, $n = 5$ ES(−) vs. 0.58 ± 0.05, $n = 5$ ES(+), $p < .01$; Fig. 5F). By 6 weeks of therapy, the increased left ventricular volume was normalized (i.e., 88.0 ± 6.8 *p*l, $n = 5$ ES(−) vs. 30.4 ± 6.8 μl, $n = 5$ ES(+), $p < .01$; Fig. 5G). Functional improvement detected by echocardiography was supported by favorable structural remodeling, demonstrated by marked reduction in cardiac hypertrophy (Fig. 5H) in response to stem cell therapy (i.e., heart weight: 301.8 ± 21.9 mg, $n = 5$ ES(−) vs. 167.8 ± 7.0 mg, $n = 5$ ES(+), $p < .01$; Fig. 5I). Thus, bioinformatic interrogation for prediction of specific cardiomyopathic traits of cardiac function and structure in response to cell therapy were validated by in vivo echocardiography and ex vivo pathology.

Stem Cell Therapy Prioritizes a Cardio-Regenerative Proteome Module

Iterative systems interrogation enables unbiased identification and stratification of functional categories emerging from a perturbed proteome [36]. 2D gel analysis revealed that stem cell therapy induced 28 significantly altered protein species (Fig. 6A). Gel-to-gel reproducibility indicated high correlation of average normalized intensities of matching protein species (Fig. 6A, inset). Mass spectometric analysis of protein species altered by cell therapy resolved 61 unique protein identities (Fig. 6B; Supporting Information Table S1 and Table S4). Proteins integrated into an organized network of 120 nodes linked by 560 edges (Fig. 7A). A nonrandom, scale-free topology was deduced based on network degree distribution properties (Fig. 7B). Ontological assessment of the stem cell-induced interactome against curated biological processes extracted categorically overrepresented functions, with “cardiovascular system development” prioritized among the ranking of all developmental functions (Fig. 7C). In contrast, “cardiovascular system development” was not prioritized in the untreated cardiomyopathic network, and was reduced in significance by more than one order of magnitude, that is, $p = 1.98 \times 10^{-5}$ and 4.14×10^{-4} relative to cell therapy, indicating a cardio-rejuvenative substrate induced by stem cell intervention. Thus, iterative proteome-wide network resolution unmasked a regenerative signature induced by embryonic stem cell treatment of failing heart in the context of K_{ATP} channel-deficient cardiomyopathy.

DISCUSSION

Transplantation of stem cells shows promise in the treatment of cardiovascular disease, yet the molecular foundation that underlies repair remains largely unknown [16, 17]. The present study deciphers the proteomic landscape induced by embryonic stem cell intervention in a surrogate of type 1O human genetic dilated cardiomyopathy produced by stress in the setting of K_{ATP} channel deficiency. In this nonischemic heart failure model, using proteomics and network analysis, we demonstrate that pluripotent stem cell therapy downgrades adverse consequences of disease, as a result of global remodeling of the pathologic heart, inducing a distinct cardio-regenerative proteome featuring a prioritized cardiovascular development signature. The resolved, stem cell-dependent subproteome identifies a previously undefined regenerative substrate of heart failure repair.

Systems Pathology of Genetic Cardiomyopathy

Traditional means of risk assessment have focused on single candidate pathways [53]. The emergence of systems approaches now enables unbiased, integrative surveys of complex disease states [54–56]. In this regard, proteome-wide profiling provides a high-throughput/high-specificity platform to extract disease processes at a global scale [57, 58]. As applied in this study, proteomics in conjunction with network-based systems analysis incorporates all measured changes for in silico bioinformatic interrogation of disease and therapy phenotypes, avoiding potential bias that may be introduced by selectively focusing only on a particular class of altered protein, for example, those of greatest differential expression, or selection of suspected candidate proteins regardless of observed change in expression [59]. Multiple etiologies cause cardiomyopathies, with complex disease phenotypes arising through interactions between individual genetic make-up and environmental stress challenges [1–8, 60]. Moreover, cardiomyopathic triggers may corrupt the resident cardiac stem cell compartment jeopardizing the innate repair potential of the myocardium [23]. Here, proteomic analysis was implemented within an established paradigm of genetic cardiomyopathy, that is, the stressed K_{ATP} channel knockout model that recapitulates salient traits of human disease [24, 40]. The *KCNJ11* null mutant under imposed hemo-dynamic load demonstrates compromised contractility and ventricular dilation predisposing to premature death [40], features of the life-threatening cardiomyopathic CMD 1O syndrome associated with mutations in genes encoding for subunits of the K_{ATP} channel [8, 11]. Compared to nonfailing unstressed counterparts, failing K_{ATP} channel knockout hearts, exposed to the stress of chronic pressure overload, displayed a pronounced rearrangement of the cardiac proteome. The primary impact of the 109 significantly altered protein changes centered on energy metabolism with 70 unique proteins stratified into the “cellular metabolism” category, consistent with impaired metabolic homeostasis a recognized hallmark underlying initiation and maintenance of heart failure [9, 61–64]. Accumulation of defects along energetic pathways precipitates failure of the whole cardiac bioenergetic system leading to myocardial dysfunction [61]. The present systems pathology approach thus pinpoints identities of affected proteins, revealing the broad landscape underlying the K_{ATP} channel-deficient CMD1O cardiomyopathic proteome.

Stem Cell Therapy Restructures Cardiomyopathic Proteome

Current pharmacotherapy for dilated cardiomyopathy is largely designed to address symptom reduction or limit disease progression [3, 7, 65]. Targeting heart repair mandates a regimen with the capacity to replace dysfunctional heart muscle [17, 66], as recently demonstrated with tissue reconstruction by stem cell-based therapy in the setting of cardiomyopathy [23, 24]. Beyond dissecting the pathobiological complexity of disease, proteomic approaches could decode responses triggered by applied therapies and ensure a holistic perspective by network integration [35, 67]. It should be noted, however, that global relationships between protein targets and treatment algorithms remain largely uncharacterized [68]. In this first proteomic examination of the large-scale impact of stem cell therapy in disease, a comprehensive protein registry was collected at 6 weeks post-transplantation of embryonic stem cells into failing K_{ATP} channel-deficient hearts. Cell intervention was found to produce a significant imprint upon the host myocardium, particularly affecting components of energetic metabolism and metabolism-related infrastructure. Operating as part of highly interconnected cellular networks, the stem cell-dependent interactome was encompassed within a nonstochastic network of protein–protein relationships that diverged from that of the stem cell-independent counterpart. These data indicate that embryonic stem cell treatment orchestrated a wide spectrum of change that collectively restructured the diseased proteome architecture underlying the active process of repair.

Cardio-Regenerative Network Signature Underlies Stem Cell-Based Repair

The processes of protein identification, ontological stratification, and iterative interrogation create a systems tool to project phenotypic outcome [38, 69]. Cytotherapy here canceled six of seven prominent cardiac-specific adverse outcomes prioritized by disease, providing a new proteome identity to the healing myocardium. Verifying bioinformatic output, independent functional and structural measurements documented increased ejection fraction and fractional shortening, reduced ventricular dilation and reversal of cardiomegaly affirming benefit in vivo. Moreover, the in silico prediction of overrepresentation of fibrosis was experimentally verified in tissue samples, and was significantly reduced in treated versus untreated hearts [24]. This unprecedented proteomic perspective offers thereby a reliable resource to diagnose a reparative response at a systems level. Further deconvolution of the stem cell-dependent subproteome exposed a cardiovascular development-enriched module absent from untreated cohorts. In line with the documented formation of new cardiac tissue and cell cycle activation in ~15% of cells within embryonic stem cell-treated cardiac tissue, normalizing sarcomeric and gap junction organization [24], the present findings map a dynamic host–graft interaction that transitions the proteome from a diseased towards a regenerative state. The multifaceted nature of regenerative repair mechanisms includes contributions from both endogenous and exogenous sources [70]. Notwithstanding, here the source of resolved proteins could not be distinguished as transplanted cells came from the same species as the endogenous tissue to avoid rejection and maximize engraftment.

CONCLUSION

Current experience with stem cell-based therapy has been primarily focused on ischemic forms of heart disease, whereas less is known of the potential benefit in the setting of nonischemic cardiomyopathy. Here, global protein expression profiling and comparative network analysis extracted from dilated, nonischemic cardiomyopathic ventricles distinct interactomes in the absence versus presence of embryonic stem cell treatment, establishing a proteomic fingerprint characterizing cell-based therapy in the context of K_{ATP} channel dysfunction and heart failure. The decoded proteomic profile provides a systems framework to diagnose regenerative patterns imposed by stem cell-based intervention.

Supplementary Material

Refer to Web version on PubMed Central for supplementary material.

Acknowledgments

We thank Jonathan Nesbitt (Mayo Clinic) for surgical expertise, and the Mayo Proteomics Research Center staff for guidance in mass spectrometry analysis. We are particularly grateful to Dr. Takashi Miki (Chiba University, Chiba, Japan) and Dr. Susumu Seino (Kobe University, Kobe, Japan) for the initial derivation of the Kir6.2 knockout mice. This work was supported by the National Institutes of Health (R01HL064822, R01HL083439, T32HL007111), Marriott Heart Disease Research Program, and Mayo Clinic. J.Z.L. holds a Mayo Graduate School fellowship. D.K.A. is the recipient of a Marriott Individualized Medicine Career Development Award. S.Y. is the recipient of an American Society for Clinical Pharmacology and Therapeutics Young Investigator Award and a Marriott Mitochondrial Medicine Award. T.J.N. is a recipient of a PhRMA Foundation Faculty Development Award. A.T. holds the Marriott Family Professorship in Cardiovascular Research at Mayo Clinic.

REFERENCES

1. Towbin JA, Bowles NE. The failing heart. Nature. 2002; 415:227–233. [PubMed: 11805847]
2. Hershberger RE, Lindenfeld J, Mestroni L, et al. Genetic evaluation of cardiomyopathy: A Heart Failure Society of America practice guideline. J Card Fail. 2009; 15:83–97. [PubMed: 19254666]

3. Luk A, Ahn E, Soor GS, et al. Dilated cardiomyopathy: A review. J Clin Pathol. 2009; 62:219–225. [PubMed: 19017683]
4. Chien KR. Genomic circuits and the integrative biology of cardiac diseases. Nature. 2000; 407:227–232. [PubMed: 11001065]
5. Ahmad F, Seidman JG, Seidman CE. The genetic basis for cardiac remodeling. Annu Rev Genomics Hum Genet. 2005; 6:185–216. [PubMed: 16124859]
6. Olson, TM. Monogenic dilated cardiomyopathy. In: Walsh, RA., editor. Molecular Mechanisms of Cardiac Hypertrophy and Failure. 1st ed.. Boca Raton, Florida: Taylor & Francis; 2005. p. 525-540.
7. Hershberger RE, Cowan J, Morales A, et al. Progress with genetic cardiomyopathies: Screening, counseling, and testing in dilated, hy-pertrophic, and arrhythmogenic right ventricular dysplasia/ cardiomyopathy. Circ Heart Fail. 2009; 2:253–261. [PubMed: 19808347]
8. Bienengraeber M, Olson TM, Selivanov VA, et al. ABCC9 mutations identified in human dilated cardiomyopathy disrupt catalytic K_{ATP} channel gating. Nat Genet. 2004; 36:382–387. [PubMed: 15034580]
9. Kane GC, Liu XK, Yamada S, et al. Cardiac K_{ATP} channels in health and disease. J Mol Cell Cardiol. 2005; 38:937–943. [PubMed: 15910878]
10. Reyes S, Park S, Johnson BD, et al. K_{ATP} channel Kir6.2 E23K variant overrepresented in human heart failure is associated with impaired exercise stress response. Hum Genet. 2009; 126:779–789. [PubMed: 19685080]
11. Olson TM, Terzic A. Human K_{ATP} channelopathies: Diseases of metabolic homeostasis. Pflugers Arch Eur J Physiol. 2010; 460:295–306. [PubMed: 20033705]
12. Ashrafian H, Watkins H. Cardiomyopathies: Therapeutics based on molecular phenotype. J Am Coll Cardiol. 2007; 49:1251–1264. [PubMed: 17394955]
13. Hunt SA, Abraham WT, Chin MH, et al. 2009 focused update incorporated into the ACC/AHA 2005 Guidelines for the Diagnosis and Management of Heart Failure in Adults: A report of the American College of Cardiology Foundation/American Heart Association Task Force on Practice Guidelines: Developed in collaboration with the International Society for Heart and Lung Transplantation. Circulation. 2009; 119:e391–e479. [PubMed: 19324966]
14. Dimmeler S, Zeiher AM, Schneider MD. Unchain my heart: The scientific foundations of cardiac repair. J Clin Invest. 2005; 115:572–583. [PubMed: 15765139]
15. Passier R, van Laake LW, Mummery CL. Stem cell-based therapy and lessons from the heart. Nature. 2008; 453:322–329. [PubMed: 18480813]
16. Segers VF, Lee RT. Stem cell therapy for cardiac disease. Nature. 2008; 451:937–942. [PubMed: 18288183]
17. Hansson EM, Lindsay ME, Chien KR. Regeneration next: Toward heart stem cell therapeutics. Cell Stem Cell. 2009; 5:364–377. [PubMed: 19796617]
18. Nelson TJ, Behfar A, Yamada S, et al. Stem cell platforms for regenerative medicine. Clin Transl Sci. 2009; 2:222–227. [PubMed: 19779576]
19. Anversa P, Kajstura J, Leri A, et al. Life and death of cardiac stem cells: A paradigm shift in cardiac biology. Circulation. 2006; 113:1451–1463. [PubMed: 16549650]
20. Torella D, Ellison GM, Méndez-Ferrer S, et al. Resident human cardiac stem cells: Role in cardiac cellular homeostasis and potential for myocardial regeneration. Nat Clin Pract Cardiovasc Med. 2006; 3 suppl 1:8–13.
21. Kajstura J, Hosoda T, Bearzi C, et al. The human heart: A self-renewing organ. Clin Transl Sci. 2008; 1:80–86. [PubMed: 20443822]
22. Bergmann O, Bhardwaj RD, Bernard S, et al. Evidence for cardiomyocyte renewal in humans. Science. 2009; 324:98–102. [PubMed: 19342590]
23. De Angelis A, Piegari E, Cappetta D, et al. Anthracycline cardiomyopathy is mediated by depletion of the cardiac stem cell pool and is rescued by restoration of progenitor cell function. Circulation. 2010; 121:276–292. [PubMed: 20038740]
24. Yamada S, Nelson TJ, Crespo-Diaz RJ, et al. Embryonic stem cell therapy of heart failure in genetic cardiomyopathy. Stem Cells. 2008; 26:2644–2653. [PubMed: 18669912]

25. Hodgson DM, Behfar A, Zingman LV, et al. Stable benefit of embryonic stem cell therapy in myocardial infarction. Am J Physiol Heart Circ Physiol. 2004; 287:H471–H479. [PubMed: 15277190]
26. Me´nard C, Hage`ge AA, Agbulut O, et al. Transplantation of cardiac-committed mouse embryonic stem cells to infarcted sheep myocardium: A preclinical study. Lancet. 2005; 366:1005–1012. [PubMed: 16168783]
27. Kolossov E, Bostani T, Roell W, et al. Engraftment of engineered ES cell-derived cardiomyocytes but not BM cells restores contractile function to the infarcted myocardium. J Exp Med. 2006; 203:2315–2327. [PubMed: 16954371]
28. Chung S, Dzeja PP, Faustino RS, et al. Mitochondrial oxidative metabolism is required for the cardiac differentiation of stem cells. Nat Clin Pract Cardiovasc Med. 2007; 4 suppl 1:60–67. [PubMed: 17245398]
29. Laflamme MA, Chen KY, Naumova AV, et al. Cardiomyocytes derived from human embryonic stem cells in pro-survival factors enhance function of infarcted rat hearts. Nat Biotechnol. 2007; 25:1015–1024. [PubMed: 17721512]
30. Kehat I, Khimovich L, Caspi O, et al. Electromechanical integration of cardiomyocytes derived from human embryonic stem cells. Nat Bio-technol. 2004; 22:1282–1289.
31. Baba S, Heike T, Yoshimoto M, et al. Flk1^{+} cardiac stem/progenitor cells derived from embryonic stem cells improve cardiac function in a dilated cardiomyopathy mouse model. Cardiovasc Res. 2007; 76:119–131. [PubMed: 17560966]
32. Behfar A, Perez-Terzic C, Faustino RS, et al. Cardiopoietic programming of embryonic stem cells for tumor-free heart repair. J Exp Med. 2007; 204:405–420. [PubMed: 17283208]
33. Nelson TJ, Martinez-Fernandez A, Yamada S, et al. Repair of acute myocardial infarction with human stemness factors induced pluirpotent stem cells. Circulation. 2009; 120:408–416. [PubMed: 19620500]
34. Baraba´si AL, Oltvai ZN. Network biology: Understanding the cell's functional organization. Nat Rev Genet. 2004; 5:101–113. [PubMed: 14735121]
35. Weston AD, Hood L. Systems biology, proteomics, and the future of health care: Toward predictive, preventative, and personalized medicine. J Proteome Res. 2004; 3:179–196. [PubMed: 15113093]
36. Arrell DK, Niederländer NJ, Faustino RS, et al. Cardioinductive network guiding stem cell differentiation revealed by proteomic cartography of tumor necrosis factor α-primed endodermal secretome. Stem Cells. 2008; 26:387–400. [PubMed: 17991915]
37. Van Hoof D, Heck AJ, Krijgsveld J, et al. Proteomics and human embryonic stem cells. Stem Cell Res. 2008; 1:169–182. [PubMed: 19383398]
38. Arrell DK, Zlatkovic J, Kane GC, et al. ATP-sensitive K^{+} channel knockout induces cardiac proteome remodeling predictive of heart disease susceptibility. J Proteome Res. 2009; 8:4823–4834. [PubMed: 19673485]
39. Kane GC, Behfar A, Dyer RB, et al. KCNJ11 Gene knockout of the Kir62 K_{ATP} channel causes maladaptive remodeling and heart failure in hypertension. Hum Mol Genet. 2006; 15:2285–2297. [PubMed: 16782803]
40. Yamada S, Kane GC, Behfar A, et al. Protection conferred by myocardial ATP-sensitive K^{+} channels in pressure overload-induced congestive heart failure revealed in *KCNJ11* Kir6.2-null mutant. J Physiol. 2006; 577:1053–1065. [PubMed: 17038430]
41. Martinez-Fernandez A, Nelson TJ, Yamada S, et al. iPS programmed without c-MYC yield proficient cardiogenesis for functional heart chi-merism. Circ Res. 2009; 105:648–656. [PubMed: 19696409]
42. Yamada S, Nelson TJ, Behfar A, et al. Stem cell transplant into preim-plantation embryo yields myocardial infarction-resistant adult phenotype. Stem Cells. 2009; 27:1697–1705. [PubMed: 19544428]
43. Zlatkovic J, Arrell DK, Kane GC, et al. Proteomic profiling of K_{ATP} channel-deficient hypertensive heart maps risk for maladaptive cardiomyopathic outcome. Proteomics. 2009; 9:1314–1325. [PubMed: 19253285]

44. Arrell DK, Niederländer NJ, Perez-Terzic C, et al. Embryonic stem cell cardiac differentiation: A proteomic perspective. Adv Mol Med. 2006; 2:149–156.
45. Arrell DK, Niederländer NJ, Perez-Terzic C, et al. Pharmacoproteomics: Advancing the efficacy and safety of regenerative therapeutics. Clin Pharmacol Ther. 2007; 82:316–319. [PubMed: 17671447]
46. Perkins DN, Pappin DJC, Creasy DM, et al. Probability-based protein identification by searching sequence databases using mass spectrometry data. Electrophoresis. 1999; 20:3551–3567. [PubMed: 10612281]
47. Link AJ, Eng J, Schieltz DM, et al. Direct analysis of protein complexes using mass spectrometry. Nat Biotechnol. 1999; 17:676–682. [PubMed: 10404161]
48. Cline MS, Smoot M, Cerami E, et al. Integration of biological networks and gene expression data using Cytoscape. Nat Protoc. 2007; 2:2366–2382. [PubMed: 17947979]
49. Assenov Y, Ramírez F, Schelhorn S-E, et al. Computing topological parameters of biological networks. Bioinformatics. 2008; 24:282–284. [PubMed: 18006545]
50. Barabasí A-L, Albert R. Emergence of scaling in random networks. Science. 1999; 286:509–512. [PubMed: 10521342]
51. Jeong H, Tombor B, Albert R, et al. The large-scale organization of metabolic networks. Nature. 2000; 407:651–654. [PubMed: 11034217]
52. Newman MEJ. The structure and function of complex networks. SIAM Rev. 2003; 45:167–256.
53. Braunwald E. Biomarkers in heart failure. N Engl J Med. 2008; 358:2148–2159. [PubMed: 18480207]
54. Bell J. Predicting disease using genomics. Nature. 2004; 429:453–456. [PubMed: 15164070]
55. Arab S, Gramolini AO, Ping P, et al. Cardiovascular proteomics: Tools to develop novel biomarkers and potential applications. J Am Coll Cardiol. 2006; 48:1733–1741. [PubMed: 17084242]
56. Asakura M, Kitakaze M. Global gene expression profiling in the failing myocardium. Circ J. 2009; 73:1568–1576. [PubMed: 19638707]
57. Gstaiger M, Aebersold R. Applying mass spectrometry-based proteo-mics to genetics, genomics and network biology. Nat Rev Genet. 2009; 10:617–627. [PubMed: 19687803]
58. Merico D, Gfeller D, Bader GD. How to visually interpret biological data using networks. Nat Biotechnol. 2009; 27:921–924. [PubMed: 19816451]
59. Arrell DK, Terzic A. Network systems biology for drug discovery. Clin Pharmacol Ther. 2010; 88:120–125. [PubMed: 20520604]
60. Chien KR. Stress pathways and heart failure. Cell. 1999; 98:555–558. [PubMed: 10490095]
61. Dzeja PP, Redfield MM, Burnett JC, et al. Failing energetics in failing hearts. Curr Cardiol Rep. 2000; 2:212–217. [PubMed: 10980895]
62. Neubauer S. The failing heart: An engine out of fuel. N Engl J Med. 2007; 356:1140–1151. [PubMed: 17360992]
63. Chen CH, Budas GR, Churchill EN, et al. Activation of aldehyde dehydrogenase-2 reduces ischemic damage to the heart. Science. 2008; 321:1493–1495. [PubMed: 18787169]
64. Ping P. Getting to the heart of proteomics. N Engl J Med. 2009; 360:532–534. [PubMed: 19179323]
65. Waldman SA, Terzic A. Therapeutic targeting: A crucible for individualized medicine. Clin Pharmacol Ther. 2008; 83:651–654. [PubMed: 18425084]
66. Nelson TJ, Behfar A, Terzic A. Strategies for therapeutic repair: The "R^3" regenerative medicine paradigm. Clin Transl Sci. 2008; 1:168–171. [PubMed: 19756244]
67. Lusis AJ, Weiss JN. Cardiovascular networks. Systems-based approaches to cardiovascular disease. Circulation. 2010; 121:157–170. [PubMed: 20048233]
68. Yildirim MA, Goh KI, Cusick ME, et al. Drug-target network. Nat Biotechnol. 2007; 25:1119–1126. [PubMed: 17921997]
69. Hood L, Heath JR, Phelps ME, et al. Systems biology and new technologies enable predictive and preventative medicine. Science. 2004; 306:640–643. [PubMed: 15499008]

70. Gersh BJ, Simari RD, Behfar A, et al. Cardiac cell repair therapy: A clinical perspective. Mayo Clin Proc. 2009; 84:876–892. [PubMed: 19797777]

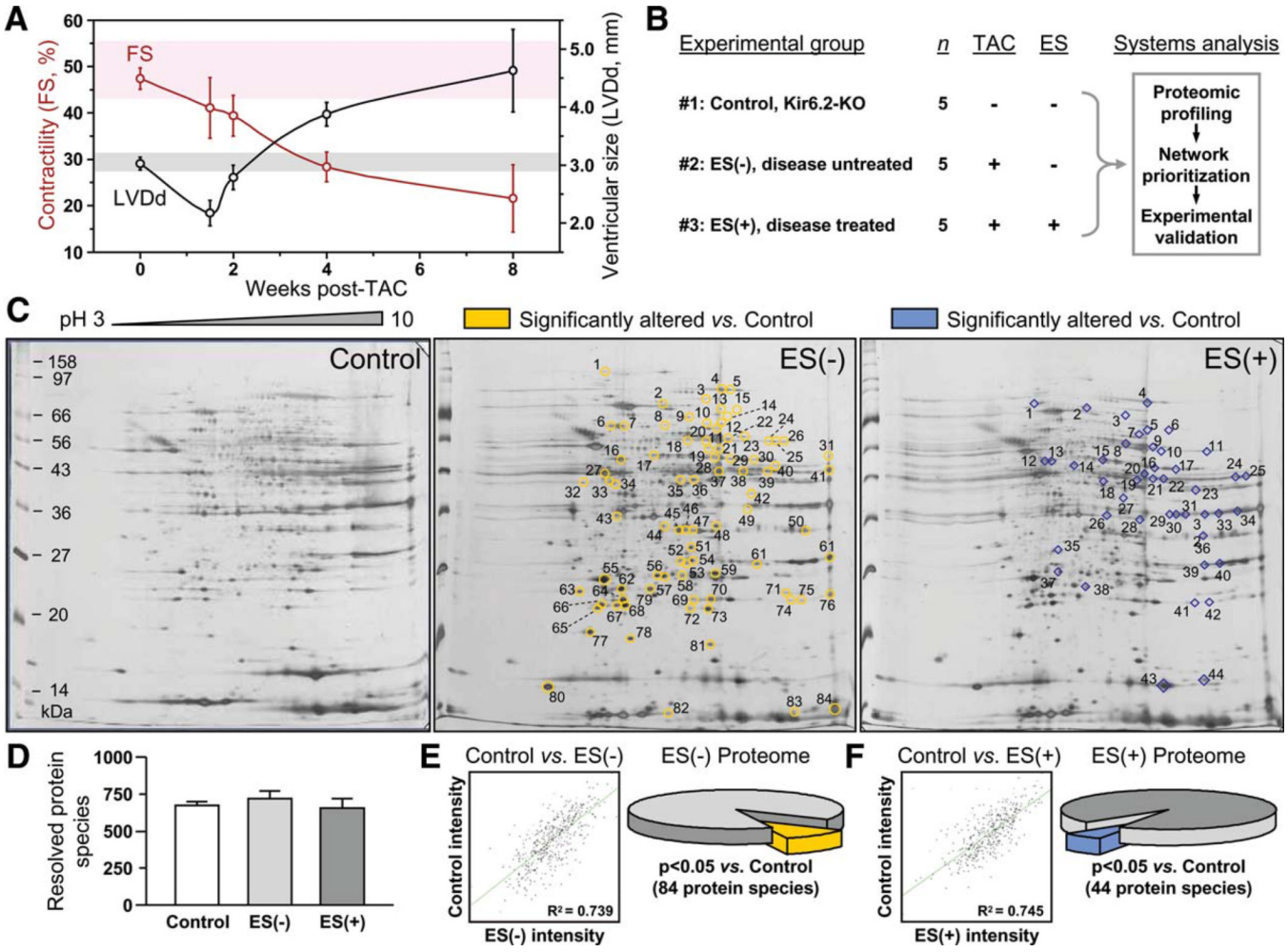

Figure 1.

Stem cell intervention remodels heart proteome in genetic dilated cardiomyopathy. (**A**): Malignant dilated cardiomyopathy in K_{ATP} channel-deficient (Kir6.2-KO) hearts under stress imposed by TAC characterized by decreased contractility (**FS**) and increased LVDd following initial compensatory hypertrophy observed at 1.5 weeks post-TAC. Shaded background indicates 95% confidence interval for FS (pink) and LVDd (gray) in age- and sex-matched Kir6.2-KO (Control) hearts. (**B**): The experimental protocol involved systems analysis combining proteomic comparison of left ventricular (LV) extracts obtained 8 weeks post-TAC from three separate experimental groups, unstressed Kir6.2-KO (#1 - Control), disease untreated TAC Kir6.2-KO [#2 – ES(−)] and disease treated TAC Kir6.2-KO [#3 – ES(+)] treated by 6 weeks of R1 embryonic stem cell therapy, followed by network analysis and in silico prioritization of proteomic findings in conjunction with in vivo and ex vivo functional validation. (**C**): Representative silver stained two-dimensional gels (pH 3–10 IEF, 12.5% SDS-PAGE) of LV tissue extracts (100 μg protein) from unstressed Kir6.2-KO (control), and from aortic-constricted untreated [ES(−)] or stem cell-treated [ES(+)] counterparts. Spots identified as differentially expressed relative to those in unstressed hearts are circled and numbered on ES(−) and ES(+) gels. (**D**): Gel reproducibility demonstrated by no significant difference in number of resolved protein species. (**E, F**): Densitometric spot quantitation, with scatter plots of average normalized intensities of matching protein spots showing correlation for control versus ES(−) and control versus ES(+) gels, and pie charts indicating significant differences in 84 and 44 protein species for

control versus ES(−) and control versus ES(+), respectively ($p < .05$). Abbreviations: ES, embryonic stem cells; FS, fractional shortening; LVDd, left ventricular end-diastolic dimension; TAC, transverse aortic constriction.

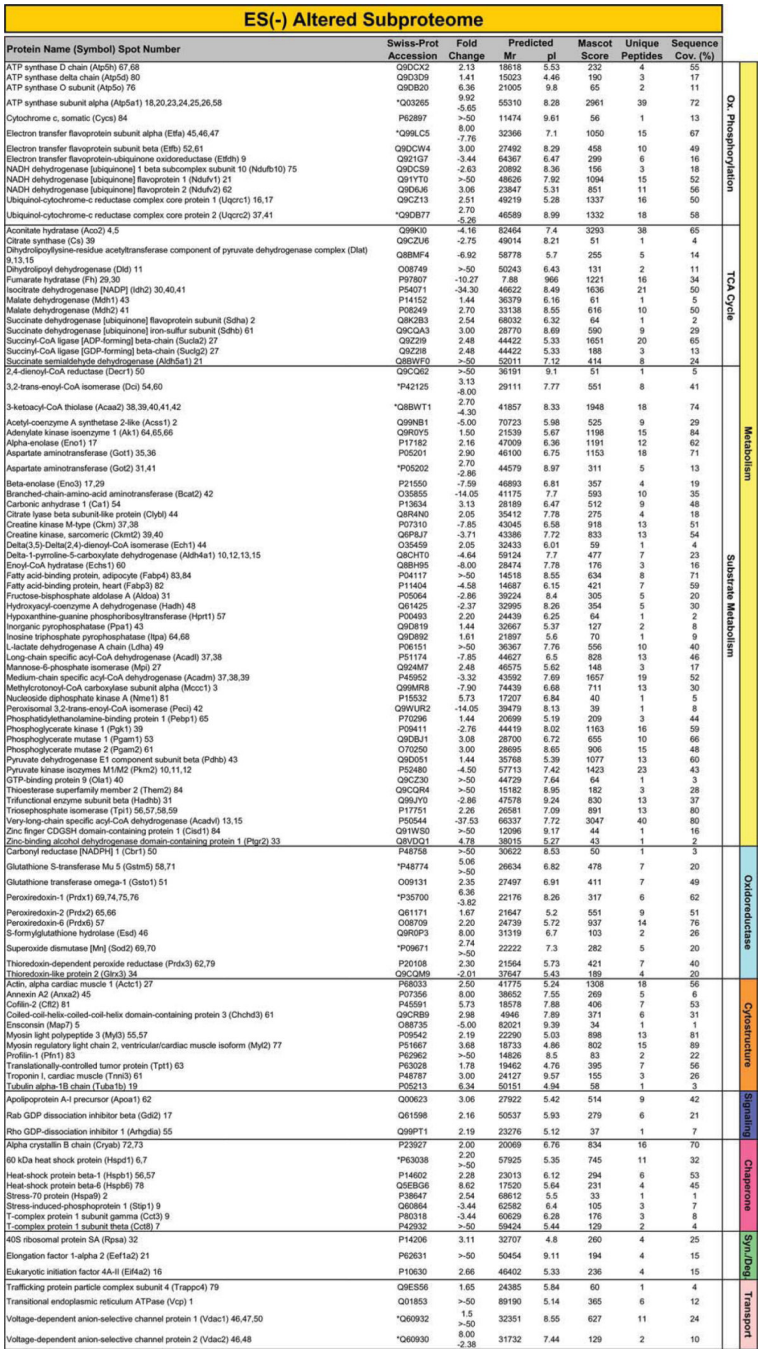

ES(-) Altered Subproteome

Protein Name (Symbol) Spot Number	Swiss-Prot Accession	Fold Change	Predicted Mr	Predicted pI	Mascot Score	Unique Peptides	Sequence Cov. (%)	
ATP synthase D chain (Atp5h) 67,68	Q9DCX2	2.13	18618	5.53	232	4	55	Ox. Phosphorylation
ATP synthase delta chain (Atp5d) 80	Q9D3D9	1.41	15023	4.46	190	3	17	
ATP synthase O subunit (Atp5o) 76	Q9DB20	6.36	21005	9.8	65	2	11	
ATP synthase subunit alpha (Atp5a1) 18,20,23,24,25,26,58	*Q03265	9.92 -5.65	55310	8.28	2961	39	72	
Cytochrome c, somatic (Cycs) 84	P62897	>-50	11474	9.61	56	1	13	
Electron transfer flavoprotein subunit alpha (Etfa) 45,46,47	*Q99LC5	8.00 -7.76	32366	7.1	1050	15	67	
Electron transfer flavoprotein subunit beta (Etfb) 52,61	Q9DCW4	3.00	27492	8.29	458	10	49	
Electron transfer flavoprotein-ubiquinone oxidoreductase (Etfdh) 9	Q921G7	-3.44	64367	6.47	299	6	16	
NADH dehydrogenase [ubiquinone] 1 beta subcomplex subunit 10 (Ndufb10) 75	Q9DCS9	-2.63	20892	8.36	156	3	18	
NADH dehydrogenase [ubiquinone] flavoprotein 1 (Ndufv1) 21	Q91YT0	>-50	48626	7.92	1094	15	52	
NADH dehydrogenase [ubiquinone] flavoprotein 2 (Ndufv2) 62	Q9D6J6	3.06	23847	5.31	851	11	56	
Ubiquinol-cytochrome-c reductase complex core protein 1 (Uqcrc1) 16,17	Q9CZ13	2.51	49219	5.28	1337	16	50	
Ubiquinol-cytochrome-c reductase complex core protein 2 (Uqcrc2) 37,41	*Q9DB77	2.70 -5.26	46589	8.99	1332	18	58	
Aconitate hydratase (Aco2) 4,5	Q99KI0	-4.16	82464	7.4	3293	38	65	TCA Cycle
Citrate synthase (Cs) 39	Q9CZU6	-2.75	49014	8.21	51	1	4	
Dihydrolipoyllysine-residue acetyltransferase component of pyruvate dehydrogenase complex (Dlat) 9,13,15	Q8BMF4	-6.92	58778	5.7	255	5	14	
Dihydrolipoyl dehydrogenase (Dld) 11	O08749	>-50	50243	6.43	131	2	11	
Fumarate hydratase (Fh) 29,30	P97807	-10.27	7.88	966	1221	16	34	
Isocitrate dehydrogenase [NADP] (Idh2) 30,40,41	P54071	-34.30	46622	8.49	1636	21	50	
Malate dehydrogenase (Mdh1) 43	P14152	1.44	36379	6.16	61	1	5	
Malate dehydrogenase (Mdh2) 41	P08249	2.70	33138	8.55	616	10	50	
Succinate dehydrogenase [ubiquinone] flavoprotein subunit (Sdha) 2	Q8K2B3	2.54	68032	6.32	64	1	2	
Succinate dehydrogenase [ubiquinone] iron-sulfur subunit (Sdhb) 61	Q9CQA3	3.00	28770	8.69	590	9	29	
Succinyl-CoA ligase [ADP-forming] beta-chain (Sucla2) 27	Q9ZZI9	2.48	44422	5.33	1651	20	65	
Succinyl-CoA ligase [GDP-forming] beta-chain (Suclg2) 27	Q9ZZI8	2.48	44422	5.33	188	3	13	
Succinate semialdehyde dehydrogenase (Aldh5a1) 21	Q8BWF0	>-50	52011	7.12	414	8	24	
2,4-dienoyl-CoA reductase (Decr1) 50	Q9DC69	>-50	36191	9.1	51	1	5	Substrate Metabolism
3,2-trans-enoyl-CoA isomerase (Dci) 54,60	*P42125	3.13 -8.00	29111	7.77	551	8	41	
3-ketoacyl-CoA thiolase (Acaa2) 38,39,40,41,42	*Q8BWT1	2.70 -4.30	41857	8.33	1948	18	74	
Acetyl-coenzyme A synthetase 2-like (Acss1) 2	Q99NB1	-5.00	70723	5.98	525	9	29	
Adenylate kinase isoenzyme 1 (Ak1) 64,65,66	Q9R0Y5	1.50	21539	5.67	1198	15	84	
Alpha-enolase (Eno1) 17	P17182	2.16	47009	6.36	1191	12	62	
Aspartate aminotransferase (Got1) 35,36	P05201	2.90	46100	6.75	1153	18	71	
Aspartate aminotransferase (Got2) 31,41	*P05202	2.70 -2.86	44579	8.97	311	5	13	
Beta-enolase (Eno3) 17,29	P21550	-7.59	46893	6.81	357	4	19	
Branched-chain-amino-acid aminotransferase (Bcat2) 42	O35855	-14.05	41175	7.7	593	10	35	
Carbonic anhydrase 1 (Ca1) 54	P13634	3.13	28189	6.47	512	9	48	
Citrate lyase beta subunit-like protein (Clybl) 44	Q8R4N0	2.05	35412	7.78	275	4	18	
Creatine kinase M-type (Ckm) 37,38	P07310	-7.85	43045	6.58	918	13	51	
Creatine kinase, sarcomeric (Ckmt2) 39,40	Q6P8J7	-3.71	43386	7.72	833	13	54	
Delta(3,5)-Delta(2,4)-dienoyl-CoA isomerase (Ech1) 44	O35459	2.05	32433	6.01	59	1	4	
Delta-1-pyrroline-5-carboxylate dehydrogenase (Aldh4a1) 10,12,13,15	Q8CHT0	-4.64	59124	7.7	477	7	23	
Enoyl-CoA hydratase (Echs1) 60	Q8BH95	-8.00	28474	7.78	176	3	16	
Fatty acid-binding protein, adipocyte (Fabp4) 83,84	P04117	>-50	14518	8.55	634	8	71	
Fatty acid-binding protein, heart (Fabp3) 82	P11404	-4.58	14687	6.15	421	7	59	
Fructose-bisphosphate aldolase A (Aldoa) 31	P05064	-2.86	39224	8.4	305	5	20	
Hydroxyacyl-coenzyme A dehydrogenase (Hadh) 48	Q61425	-2.37	32995	8.26	354	5	30	
Hypoxanthine-guanine phosphoribosyltransferase (Hprt1) 57	P00493	2.20	24439	6.25	64	1	2	
Inorganic pyrophosphatase (Ppa1) 43	Q9D819	1.44	32667	5.37	127	2	8	
Inosine triphosphate pyrophosphatase (Itpa) 64,68	Q9D892	1.61	21897	5.6	70	1	9	
L-lactate dehydrogenase A chain (Ldha) 49	P06151	>-50	36367	7.76	556	10	40	
Long-chain specific acyl-CoA dehydrogenase (Acadl) 37,38	P51174	-7.85	44627	6.5	828	13	46	
Mannose-6-phosphate isomerase (Mpi) 27	Q924M7	2.48	46575	5.62	148	3	17	
Medium-chain specific acyl-CoA dehydrogenase (Acadm) 37,38,39	P45952	-3.32	43592	7.69	1657	19	52	
Methylcrotonoyl-CoA carboxylase subunit alpha (Mccc1) 3	Q99MR8	-7.90	74439	6.68	711	13	30	
Nucleoside diphosphate kinase A (Nme1) 81	P15532	5.73	17207	6.84	40	1	5	
Peroxisomal 3,2-trans-enoyl-CoA isomerase (Peci) 42	Q9WUR2	-14.05	39479	8.13	39	1	8	
Phosphatidylethanolamine-binding protein 1 (Pebp1) 65	P70296	1.44	20699	5.19	209	3	44	
Phosphoglycerate kinase 1 (Pgk1) 39	P09411	-2.76	44419	8.02	1163	16	59	
Phosphoglycerate mutase 1 (Pgam1) 53	Q9DBJ1	3.08	28700	6.72	655	10	66	
Phosphoglycerate mutase 2 (Pgam2) 61	O70250	3.00	28695	8.65	906	15	48	
Pyruvate dehydrogenase E1 component subunit beta (Pdhb) 43	Q9D051	1.44	35768	5.39	1077	13	60	
Pyruvate kinase isozymes M1/M2 (Pkm2) 10,11,12	P52480	-4.50	57713	7.42	1423	23	43	
GTP-binding protein 9 (Ola1) 40	Q9CZ30	>-50	44729	7.64	64	1	3	
Thioesterase superfamily member 2 (Them2) 84	Q8CQR4	>-50	15182	8.95	182	3	28	
Trifunctional enzyme subunit beta (Hadhb) 31	Q99JY0	-2.86	47578	9.24	830	13	37	
Triosephosphate isomerase (Tpi1) 56,57,58,59	P17751	2.26	26581	7.09	891	13	80	
Very-long-chain specific acyl-CoA dehydrogenase (Acadvl) 13,15	P50544	-37.53	66337	7.72	3047	40	80	
Zinc finger CDGSH domain-containing protein 1 (Cisd1) 84	Q91WS0	>-50	12096	9.17	44	1	16	
Zinc-binding alcohol dehydrogenase domain-containing protein 1 (Ptgr2) 33	Q8VDQ1	4.78	38015	5.27	43	1	2	
Carbonyl reductase [NADPH] 1 (Cbr1) 50	P48758	>-50	30622	8.53	50	1	3	Oxidoreductase
Glutathione S-transferase Mu 5 (Gstm5) 58,71	*P48774	5.06 >-50	26634	6.82	478	7	20	
Glutathione transferase omega-1 (Gsto1) 51	O09131	2.35	27497	6.91	411	7	49	
Peroxiredoxin-1 (Prdx1) 69,74,75,76	*P35700	6.36 -3.82	22176	8.26	317	6	62	
Peroxiredoxin-2 (Prdx2) 65,66	Q61171	1.67	21647	5.2	551	9	51	
Peroxiredoxin-6 (Prdx6) 57	O08709	2.20	24739	5.72	937	14	76	
S-formylglutathione hydrolase (Esd) 46	Q9R0P3	8.00	31319	6.7	103	2	26	
Superoxide dismutase [Mn] (Sod2) 69,70	*P09671	2.74 >-50	22222	7.3	282	5	20	
Thioredoxin-dependent peroxide reductase (Prdx3) 62,79	P20108	2.30	21564	5.73	421	7	40	
Thioredoxin-like protein 2 (Glrx3) 34	Q9CQM9	-2.01	37647	5.43	189	4	20	
Actin, alpha cardiac muscle 1 (Actc1) 27	P68033	2.50	41775	5.24	1308	18	56	Cytostructure
Annexin A2 (Anxa2) 45	P07356	8.00	38652	7.55	269	5	6	
Cofilin-2 (Cfl2) 81	P45591	5.73	18578	7.88	406	7	53	
Coiled-coil-helix-coiled-coil-helix domain-containing protein 3 (Chchd3) 61	Q9CRB9	2.98	4946	7.89	371	6	31	
Ensconsin (Map7) 5	O88735	-5.00	82021	9.39	34	1	1	
Myosin light polypeptide 3 (Myl3) 55,57	P09542	2.19	22290	5.03	898	13	81	
Myosin regulatory light chain 2, ventricular/cardiac muscle isoform (Myl2) 77	P51667	3.68	18733	4.86	802	15	89	
Profilin-1 (Pfn1) 83	P62962	>-50	14826	8.5	83	2	22	
Translationally-controlled tumor protein (Tpt1) 63	P63028	1.78	19462	4.76	395	7	56	
Troponin I, cardiac muscle (Tnni3) 61	P48787	3.00	24127	9.57	155	3	26	
Tubulin alpha-1B chain (Tuba1b) 19	P05213	6.34	50151	4.94	58	1	3	
Apolipoprotein A-I precursor (Apoa1) 62	Q00623	3.06	27922	5.42	514	9	42	Signaling
Rab GDP dissociation inhibitor beta (Gdi2) 17	Q61598	2.16	50537	5.93	279	6	21	
Rho GDP-dissociation inhibitor 1 (Arhgdia) 55	Q99PT1	2.19	23276	5.12	37	1	7	
Alpha crystallin B chain (Cryab) 72,73	P23927	2.00	20069	6.76	834	16	70	Chaperone
60 kDa heat shock protein (Hspd1) 6,7	*P63038	2.20 >-50	57925	5.35	745	11	32	
Heat-shock protein beta-1 (Hspb1) 56,57	P14602	2.28	23013	6.12	294	6	53	
Heat-shock protein beta-6 (Hspb6) 78	Q9EBG6	8.62	17520	5.64	231	4	45	
Stress-70 protein (Hspa9) 2	P38647	2.54	68932	5.5	33	1	1	
Stress-induced-phosphoprotein 1 (Stip1) 9	Q60864	-3.44	62582	6.4	105	3	7	
T-complex protein 1 subunit gamma (Cct3) 9	P80318	-3.44	60629	6.28	176	3	8	
T-complex protein 1 subunit theta (Cct9) 7	P42932	>-50	59424	5.44	129	2	4	
40S ribosomal protein SA (Rpsa) 32	P14206	3.11	32707	4.8	260	4	25	Syn./Deg
Elongation factor 1-alpha 2 (Eef1a2) 21	P62631	>-50	50454	9.11	194	4	15	
Eukaryotic initiation factor 4A-II (Eif4a2) 16	P10630	2.66	46402	5.33	236	4	15	
Trafficking protein particle complex subunit 4 (Trappc4) 79	Q9ES56	1.65	24385	5.84	60	1	4	Transport
Transitional endoplasmic reticulum ATPase (Vcp) 1	Q01853	>-50	89190	5.14	365	6	12	
Voltage-dependent anion-selective channel protein 1 (Vdac1) 46,47,50	*Q60932	1.5 >-50	32351	8.55	627	11	24	
Voltage-dependent anion-selective channel protein 2 (Vdac2) 46,48	*Q60930	8.00 -2.38	31732	7.44	129	2	10	

Figure 2.

Identity of cardiomyopathy-induced subproteome. The 109 significantly altered proteins induced by progressive cardiomyopathy [ES(−) altered subproteome] and identified by LTQ-Orbitrap MS/MS analysis, were functionally categorized and color-coded by Swiss-Prot ontological annotation. Protein names are listed with their symbol (Swiss-Prot gene abbreviation) and spot numbers to locate corresponding 2D gel position(s) in Figure 1. Mascot score, number of unique identified peptides, % sequence cov. (coverage), predicted M_r and p*I* for each protein (following expected post-translational processing, for example, removal of a mitochondrial signal peptide), and fold change of ES(−) over control are indicated. For proteins detected in more than one spot, maximum score and corresponding

number of unique peptides are reported. Fold change was calculated as described in experimental procedures, and for proteins detected in both increasing and decreasing spots (*), both values are indicated. Abbreviations: 2D, two-dimensional; CDGSH, Unique 39 amino acid CDGSH domain [C-x-C-x2-(S/T)-x3-P-x-C-**D-G**-(S/A/T)-**H**]; ES, Embryonic stem cells; LTQ, Linear ion trap quadrupole; MS/MS, Tandem mass spectrometry; Ox., oxidative; Syn./Deg., protein synthesis/degradation; TCA cycle, tricarboxylic acid cycle.

ES(+) Altered Subproteome

Protein Name (Symbol) Spot Number(s)	Swiss-Prot Accession	Fold Change	Predicted Mr	Predicted pI	Mascot Score	Unique Peptides	Sequence Cov. (%)		
ATP synthase subunit alpha (Atp5a1) 9,10,11	Q03265	-4.47	55310	8.28	2370	33	68	Ox. Phosphorylation	Metabolism
Electron transfer flavoprotein subunit beta (Etfb) 39,40	Q9DCW4	-1.84	27492	8.29	927	14	56		
NADH dehydrogenase (Ndufs2) 14	Q91WD5	>-50	49229	5.86	1053	16	47		
NADH dehydrogenase [ubiquinone] 1 alpha subcomplex subunit 10 (Ndufa10) 18,41,42	*Q99LC3	3.56 -13.88	36943	5.96	148	3	12		
NADH-ubiquinone oxidoreductase 75 kDa subunit (Ndufs1) 1,2	*Q91VD9	3.59 -1.67	77182	5.24	2377	34	67		
Ubiquinol-cytochrome-c reductase complex core protein 1 (Uqcrc1) 12,13,14,15,16	*Q9CZ13	1.60 -5.00	49219	5.28	1547	24	59		
Ubiquinol-cytochrome-c reductase complex core protein 2 (Uqcrc2) 19,20,21,22,24,25	Q9DB77	-3.13	46589	8.99	603	10	30		
Ubiquinone biosynthesis monooxygenase COQ6 (Coq6) 15	Q8R1S0	1.64	50705	6.55	113	3	6		
Aconitate hydratase (Aco2) 4, 5	Q99KI0	>-50	82463	7.40	2653	43	65	TCA Cycle	
Citrate synthase (Cs) 20,21,22	Q9CZU6	-1.71	49014	8.21	246	5	15		
Dihydrolipoyl dehydrogenase (Dld) 8	O08749	-12.77	50242	6.43	236	5	12		
Dihydrolipoyllysine-residue acetyltransferase component of pyruvate dehydrogenase complex (Dlat) 5,6	Q8BMF4	-6.81	58778	5.70	620	11	24		
Fumarate hydratase (Fh) 15,16,17	*P97807	1.64 -3.22	49935	7.88	1233	17	60		
Isocitrate dehydrogenase [NAD] subunit alpha (Idh3a) 27	Q9D6R2	-1.55	36707	5.60	307	5	16		
Isocitrate dehydrogenase [NADP] (Idh2) 16,17,20,24,25	P54071	-2.47	46622	8.49	1556	26	53		
Malate dehydrogenase, cytoplasmic (Mdh1) 26,28	P14152	-3.70	36379	6.16	430	8	29		
Malate dehydrogenase, mitochondrial (Mdh2) 29,30,31,32,33,34	P08249	-2.39	33138	8.55	1015	15	61		
Succinyl-CoA ligase [ADP-forming] beta-chain (Sucla2) 22	Q9Z2I9	-1.87	44422	5.33	440	8	22		
Succinyl-CoA:3-ketoacid-coenzyme A transferase 1 (Oxct1) 8,9	Q9D0K2	-19.52	51876	7.01	1280	23	59		
Succinate dehydrogenase [ubiquinone] flavoprotein subunit (Sdha) 2,3	Q8K2B3	-2.31	68032	6.32	305	5	7		
2-oxoisovalerate dehydrogenase subunit alpha (Bckdha) 14	P50136	>-50	45674	6.05	604	10	32	Substrate Metabolism	
3,2-trans-enoyl-CoA isomerase (Dci) 39,40	P42125	-1.84	29110	7.77	484	8	31		
3-ketoacyl-CoA thiolase (Acaa2) 19,20,21,22,23,24,25	Q8BWT1	-3.13	41857	8.33	1446	21	72		
Acetyl-CoA acetyltransferase (Acat1) 23	Q8QZT1	-8.09	41413	8.18	992	17	51		
Acetyl-coenzyme A synthetase 2-like (Acss1) 2	Q99NB1	-1.67	70723	5.98	1135	22	45		
Acyl-coenzyme A thioesterase 9 (Acot9) 16	Q9R0X4	-4.00	48185	7.38	134	3	12		
Acyl-protein thioesterase 1 (Lypla1) 38	P97823	-2.03	24687	6.14	176	3	20		
Adenosine kinase (Adk) 14	P55264	>-50	40148	5.84	338	6	27		
Adenylyl cyclase-associated protein 1 (Cap1) 8	P40124	-12.77	51443	7.33	362	7	19		
Alpha-enolase (Eno1) 15	P17182	1.64	47009	6.36	834	11	20		
Aspartate aminotransferase, cytoplasmic (Got1) 18,19	*P05201	3.56 -9.09	46100	6.75	1390	22	68		
Aspartate aminotransferase (Got2) 19,23,25	P05202	-2.73	44579	8.97	443	7	18		
Beta-enolase (Eno3) 15,16	*P21550	1.64 -4.00	46893	6.81	1861	30	70		
Branched-chain-amino-acid aminotransferase (Bcat2) 27	O35855	-1.55	41175	7.70	579	12	44		
Carnitine O-acetyltransferase (Crat) 5	P47934	>-50	70924	8.52	71	1	1		
Creatine kinase M-type (Ckm) 19,22	P07310	-3.13	43044	6.58	1017	18	77		
Creatine kinase, sarcomeric (Ckmt2) 19,20,21,22	Q6P8J7	-2.17	43386	7.72	1389	21	62		
Delta-1-pyrroline-5-carboxylate dehydrogenase (Aldh4a1) 7	Q8CHT0	-2.51	59124	7.70	1510	26	57		
Enoyl-CoA hydratase (Echs1) 39	Q8BH95	-2.56	28474	7.78	55	1	3		
Fructose-bisphosphate aldolase A (Aldoa) 18,21,23	*P05064	3.56 -4.82	39224	8.40	1435	21	74		
Fumarylacetoacetase (Fah) 19	P35505	-9.10	46103	6.92	141	2	9		
Glyceraldehyde-3-phosphate dehydrogenase (Gapdh) 29,30,31,32,33,34	P16858	-2.39	35678	8.45	1032	14	62		
Guanine deaminase (Gda) 12,13	Q9R111	1.55	51013	5.36	414	7	18		
Hydroxyacyl-coenzyme A dehydrogenase (Hadh) 36	Q61425	-3.33	32995	8.26	698	13	55		
Isovaleryl-CoA dehydrogenase (Ivd) 19	Q9JHI5	-9.10	42971	6.29	246	4	20		
L-lactate dehydrogenase A chain (Ldha) 28	P06151	-4.48	36367	7.76	1191	18	68		
L-lactate dehydrogenase B chain (Ldhb) 29,30,31	P16125	-2.37	36441	5.70	553	9	40		
Long-chain specific acyl-CoA dehydrogenase (Acadl) 19,21,22	P51174	-3.04	44627	6.50	954	15	42		
Medium-chain specific acyl-CoA dehydrogenase (Acadm) 18,19,20,21,22	*P45952	3.56 -2.00	43592	7.69	1255	20	58		
Methylcrotonoyl-CoA carboxylase beta chain (Mccc2) 7	Q3ULD5	-2.51	58685	6.88	511	9	24		
Nicotinamide phosphoribosyltransferase (Nampt) 8	Q99KQ4	-12.77	55446	6.69	145	3	14		
Ornithine aminotransferase (Oat) 14	P29758	>-50	45790	5.73	212	3	12		
Phosphoglycerate kinase 1 (Pgk1) 20,21,22	P09411	-1.71	44419	8.02	1302	21	70		
Phosphoglycerate mutase 2 (Pgam2) 39,40	O70250	-1.84	28695	8.65	348	6	25		
Propionyl-CoA carboxylase alpha chain (Pcca) 2	Q91ZA3	-1.67	75158	6.13	2494	31	65		
Pyruvate dehydrogenase E1 component alpha subunit (Pdha1) 19,20	P35486	-2.07	40180	6.78	399	7	21		
Pyruvate dehydrogenase protein X component (Pdhx) 35	Q8BKZ9	9.53	47948	5.82	125	2	6		
Pyruvate kinase isozymes M1/M2 (Pkm2) 7	P52480	-2.51	57713	7.42	1618	26	53		
Short-chain specific acyl-CoA dehydrogenase (Acads) 18	Q07417	3.56	42231	7.12	318	6	25		
Trifunctional enzyme subunit beta (Hadhb) 12,15	Q99JY0	1.62	47578	9.24	420	8	20		
Triosephosphate isomerase (Tpi1) 37	P17751	2.50	26581	7.09	224	4	20		
UTP--glucose-1-phosphate uridylyltransferase (Ugp2) 8,9,10	Q91ZJ5	-12.77	56848	7.17	788	14	47		
Very-long-chain specific acyl-CoA dehydrogenase (Acadvl) 5,6	P50544	-6.81	66337	7.72	2805	46	84		
Aldose reductase (Akr1b1) 29,30,31	P45376	-2.37	35601	6.79	168	3	9	Oxidoreductase	
C-terminal-binding protein 1 (Ctbp1) 15	O88712	1.64	47744	6.28	64	1	4		
Glutathione S-transferase A4 (Gsta4) 38	P24472	-2.03	25563	6.77	50	1	50		
Glyoxylate reductase/hydroxypyruvate reductase (Grhpr) 26	Q91Z53	-3.27	35328	7.57	102	2	6		
L-2-hydroxyglutarate dehydrogenase (L2hgdh) 20	Q91YP0	-2.10	45664	8.01	201	3	10		
Peroxiredoxin-1 (Prdx1) 41,42	P35700	-13.88	22176	8.26	343	6	46		
Peroxiredoxin-5 (Prdx5) 44	P99029	-20.67	17014	7.70	587	11	56		
Sepiapterin reductase (Spr) 37	Q64105	2.50	27883	5.59	414	7	40		
Thioredoxin reductase 2 (Txnrd2) 8	Q9JLT4	-12.77	52886	7.09	179	4	8		
Thioredoxin-dependent peroxide reductase (Prdx3) 38	P20108	-2.03	21564	5.73	301	6	24		
Actin, alpha cardiac muscle 1 (Actc1) 22	P68033	-1.87	41774	5.24	303	5	25	Cytostructure	
Annexin A2 (Anxa2) 27	P07356	-1.55	38545	7.53	63	1	2		
Coiled-coil-helix-coiled-coil-helix domain-containing protein 3 (Chchd3) 39	Q9CRB9	-2.56	26334	8.56	87	2	14		
Cat eye syndrome critical region protein 5 homolog precursor (Cecr5) 18	Q91WM2	3.56	44930	7.35	57	1	5	Signaling	
Leucine zipper-EF-hand-containing transmembrane protein 1 (Letm1) 4	Q9Z2I0	-12.20	70684	5.33	47	1	1		
Mitochondrial inner membrane protein (Immt) 3	Q8CAQ8	>-50	83900	6.18	730	15	27		
Prohibitin (Phb) 35	P67778	9.53	29820	5.57	368	8	37		
60 kDa heat shock protein (Hspd1) 7	P63038	-2.51	57925	5.35	174	5	12	Chaperone	
Heat shock cognate 71 kDa protein (Hspa8) 3	P63017	>-50	70871	5.37	283	5	13		
Heat-shock protein beta-1 (Hspb1) 37	P14602	2.50	23013	6.12	564	11	57		
Stress-70 protein (Hspa9) 2	P38647	-1.67	68612	5.50	252	5	8		
T-complex protein 1 subunit epsilon (Cct5) 7	P80316	-2.51	59492	5.72	65	1	2		
Eukaryotic initiation factor 4A-I (Eif4a1) 12	P60843	1.57	46153	5.32	414	7	26	Syn./Degr.	
Eukaryotic initiation factor 4A-II (Eif4a2) 13	P10630	1.54	46402	5.33	442	7	27		
Eukaryotic translation initiation factor 3 subunit 5 (Eif3f) 12	Q9DCH4	1.57	38000	5.33	191	3	10		
Proliferation-associated protein 2G4 (Pa2g4) 15	P50580	1.64	43567	6.40	121	3	10		
Proteasome activator complex subunit 2 (Psme2) 35	P97372	9.53	26926	5.55	133	3	14		
Chloride intracellular channel protein 4 (Clic4) 35	Q9QYB1	9.53	28597	5.45	116	2	12	Transport	
Myoglobin (Mb) 43,44	P04247	-6.00	16938	7.23	965	15	93		
Selenium-binding protein 1 (Selenbp1) 10	P17563	-7.21	52514	5.87	306	6	18		

Figure 3.

Identity of cardiomyopathic subproteome following stem cell therapy. The 93 significantly altered proteins induced by stem cell therapy in the setting of dilated cardiomyopathy [ES(+) altered subproteome], and identified by LTQ-Orbitrap MS/MS analysis, were functionally categorized and color-coded by Swiss-Prot ontological annotation. Protein names are listed with their symbol (Swiss-Prot gene abbreviation) and spot numbers to locate corresponding 2D gel position(s) in Figure 1. Mascot score, number of unique identified peptides, % sequence cov. (coverage), predicted M_r and p*I* for each protein (following expected post-translational processing, for example, removal of a mitochondrial signal peptide), and fold change of ES(+) over control are indicated. For proteins detected in more than one spot,

maximum score and corresponding number of unique peptides are reported. Fold change was calculated as described in experimental procedures, and for proteins detected in both increasing and decreasing spots (*), both values are indicated. Abbreviations: 2D, two-dimensional; Ox., oxidative; Syn./Deg., protein synthesis/ degradation; TCA cycle, tricarboxylic acid cycle.

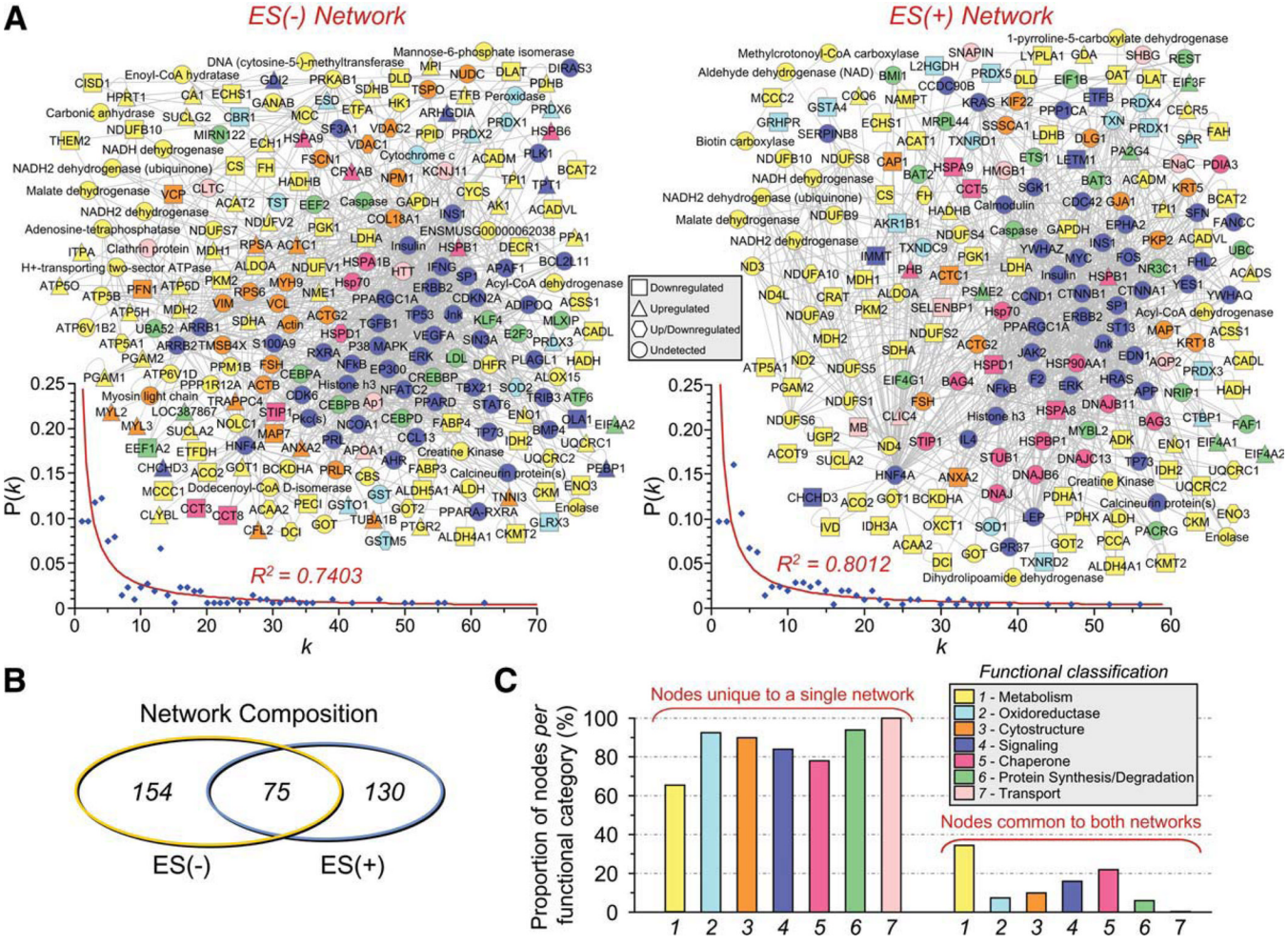

Figure 4.

Stem cell therapy transforms the cardiomyopathy-associated protein interaction network. (**A**): The 109 ES(−) and 93 ES(+) differentially expressed proteins were submitted to IPA as focus nodes, generating broader interaction networks of 229 and 205 proteins, respectively. Proteins are designated by symbols corresponding to Swiss-Prot gene abbreviations or by family name for nodes representing protein families, and are colored by the functional ontology detailed in Figures 2 and 3, with node shape indicating directionality of focus protein expression change (legend) and nodes common to both networks maintained in the same spatial location. Plots of degree distribution [P(*k*)] versus degree (*k*) followed power law distributions, where $P(k) \sim k^{-\gamma}$, with $\gamma = 1.55 \pm 0.04$ for ES(−) and 1.57 ± 0.04 for ES(+) networks, respectively, indicating scale-free, nonstochastic network architecture. (**B**): Limited overlap was found between ES(−) and ES(+) networks (total unique and common nodes indicated), with (**C**) the majority of proteins from each functional category residing within only one of the two networks. Abbreviations: ES, embryonic stem cells; P(*k*), degree distribution; *k*, node degree.

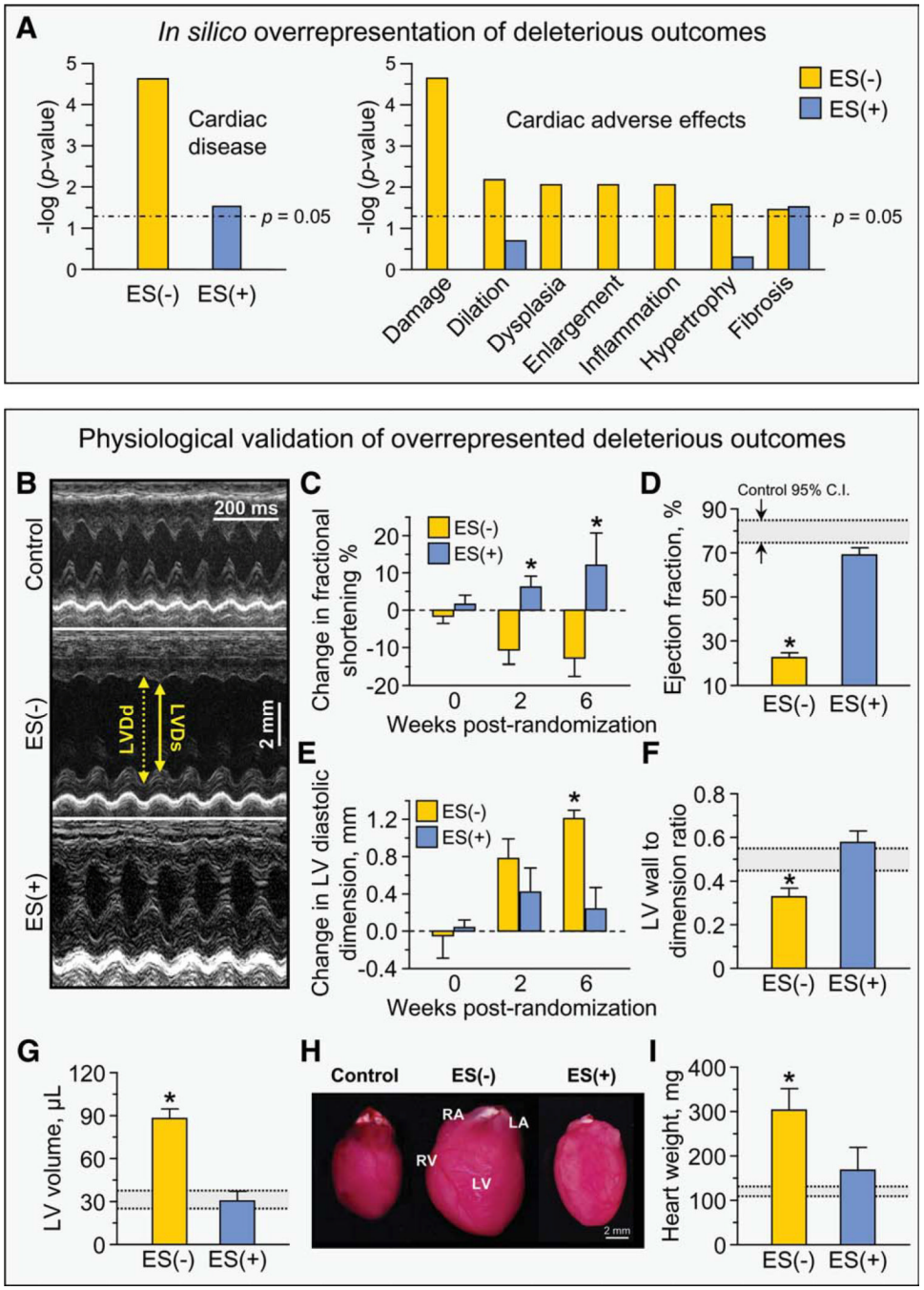

Figure 5.

Stem cell-dependent demotion of disease-associated adverse effects. (**A**): Bioinformatic interrogation of the ES(−) and ES(+) networks within Ingenuity Pathways Knowledge Base for deleterious outcomes indicated that significant overrepresentation of “Cardiac disease” within the ES(−) network was reduced by three orders of magnitude in the ES(+) network (left panel). Screening against Ingenuity toxicological pathways further indicated seven adverse effects in the ES(−) subproteome, all of which were cardiac specific, that is, damage, dilation, dysplasia, enlargement, inflammation, hypertrophy and fibrosis, and nearly all were abolished in the ES(+) subproteome (right panel). (**B**): Echocardio-graphic measurements indicated that (**C**) LV fractional shortening, (**D**) LV ejection fraction, (**E**) LV

diastolic dimension, (**F**) LV wall to dimension ratio, and (**G**) LV end-diastolic volume were all significantly worsened by pressure overload but returned to prestress levels following 6 weeks of cell therapy. (**H–I**): Measurement of hearts on autopsy indicated that the significant increase in heart mass imposed by pressure overload was reversed by cell therapy. Collectively, these parameters demonstrated cell therapy-induced improvement in myocardial contractile performance, reduction in LV size and decreased cardiac damage (*, $p < .01$ ES(−) versus ES(+) and ES(−) versus control, with control indicated by 95% C.I. in gray as noted in panel (**D**). Abbreviations: C.I., confidence intervals; ES, embryonic stem cells; LA, left atrium; LV, left ventricle; LVDd, left ventricular end-diastolic dimension; LVDs, left ventricular end-systolic dimension; RA, right atrium; RV, right ventricle.

A

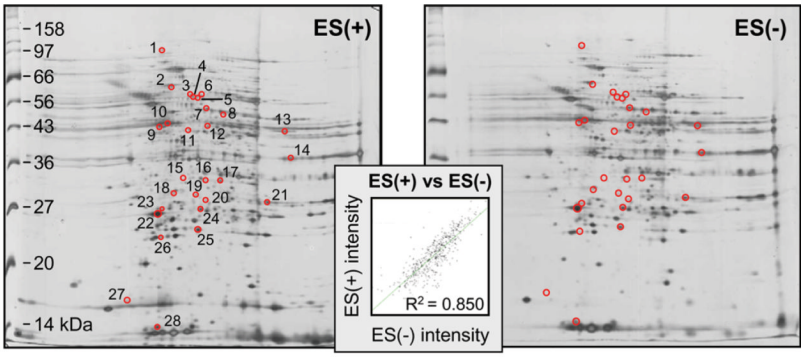

B

Protein Name (Symbol) Spot Number(s)	Swiss-Prot Accession	Fold Change	Predicted Mr	Predicted pI	Mascot Score	Unique Peptides	Sequence Cov. (%)		
ATP synthase D chain (Atp5h) 27	Q9DCX2	2.70	18618	5.53	60	1	24	Ox. Phosphorylation	Metabolism
ATP synthase subunit alpha (Atp5a1) 3,4	Q03265	-4.43	55310	8.28	325	6	16		
Electron transfer flavoprotein subunit alpha (Etfa) 19	Q99LC5	4.00	32366	7.10	363	7	43		
Electron transfer flavoprotein subunit beta (Etfb) 23	Q9DCW4	2.30	27492	8.29	465	8	36		
NADH-ubiquinone oxidoreductase 75 kDa subunit (Ndufs1) 1	Q91VD9	8.24	77182	5.24	2029	31	60		
Ubiquinol-cytochrome-c reductase complex core protein 2 (Uqcrc2) 9	Q9DB77	-2.80	46589	8.99	45	1	3		
Malate dehydrogenase (Mdh2) 15	P08249	-2.20	33138	8.55	248	6	26	TCA Cycle	
Pyruvate dehydrogenase [lipoamide] kinase isozyme 4 (Pdk4) 10	O70571	1.67	44033	6.14	272	5	36		
Succinyl-CoA ligase [ADP-forming] beta-chain (Sucla2) 9	Q9Z2I9	-2.80	44422	5.33	729	9	37		
Alpha-enolase (Eno1) 6,7	P17182	-2.13	47010	6.36	1764	22	77	Substrate Metabolism	
Beta-enolase (Eno3) 6,7	P21550	-2.13	46894	6.81	793	12	49		
Creatine kinase M-type (Ckm) 8, 9	*P07310	2.25 -2.78	43045	6.58	228	3	29		
Glyceraldehyde-3-phosphate dehydrogenase (Gapdh) 15	P16858	-2.20	35679	8.45	497	8	39		
Isovaleryl-CoA dehydrogenase (Ivd) 10	Q9JHI5	1.67	42971	6.29	1297	20	63		
Long-chain specific acyl-CoA dehydrogenase (Acadl) 8	P51174	2.25	44627	6.50	46	1	12		
Medium-chain specific acyl-CoA dehydrogenase (Acadm) 11	P45952	-6.55	43593	7.69	661	13	50		
Mitochondrial-processing peptidase alpha subunit (Pmpca) 3	Q9DC61	-4.16	54713	5.85	125	3	19		
Short-chain specific acyl-CoA dehydrogenase (Acads) 12	Q07417	>-50	42231	7.12	41	1	14		
Trifunctional purine biosynthetic protein adenosine-3 (Gart) 5	Q64737	5.22	45652	5.97	65	2	6		
Aldehyde dehydrogenase (Aldh2) 5	P47738	5.22	54375	6.05	175	4	25	Oxidoreductase	
Alpha-aminoadipic semialdehyde dehydrogenase (Aldh7a1) 3,4	Q9DBF1	-4.43	55513	5.99	110	2	6		
Glutathione peroxidase 1 (Gpx1) 28	P11352	-1.60	22268	6.74	214	5	33		
Peroxiredoxin-2 (Prdx2) 27	Q61171	2.70	21647	5.20	48	1	14		
Peroxiredoxin-6 (Prdx6) 26	O08709	-1.75	24739	5.72	102	2	16		
Thioredoxin-dependent peroxide reductase (Prdx3) 12	P20108	>-50	21564	5.73	166	3	14		
Actin, alpha cardiac muscle 1 (Actc1) 8,9	*P68033	2.25 -2.78	41785	5.23	1318	24	78	Cytostructure	
Actin, cytoplasmic 1 (Actb) 9	P60710	-2.80	41605	5.29	1149	19	70		
Myoglobin (Mb) 30, 31	P04247	-3.33	16938	7.23	842	14	83		
Myosin light polypeptide 3 (Myl3) 24,25	P09542	-1.60	22290	5.03	1445	18	86		
Protein FAM82B (Fam82b) 22	Q9DCV4	-4.40	35000	8.85	466	10	34		
Septin-2 (Sept2) 10	P42208	1.67	41525	6.10	99	2	13		
Syntaxin-binding protein 2 (Stxbp2) 24	Q64324	-1.60	66315	6.28	32	1	4		
Tropomodulin-1 (Tmod1) 8	P49813	2.25	40484	5.02	95	1	8		
Troponin I, cardiac muscle (Tnni3) 20	P48787	-2.50	24127	9.57	74	2	20		
Tubulin alpha-1B chain (Tuba1b) 2	P05213	-4.00	50151	4.94	97	1	18		
GTPase IMAP family member 4 (Gimap4) 12	Q99JY3	>-50	24554	6.53	45	1	9	Signaling	
Galectin-1 (Lgals1) 31	P16045	-3.33	14734	5.32	521	7	58		
Prohibitin (Phb) 20	P67778	-2.50	29820	5.57	168	5	39		
Protein NDRG2 (Ndrg2) 8	Q9QYG0	2.25	40789	5.23	210	5	29		
Rho GDP-dissociation inhibitor 1 (Arhgdia) 24,25	Q99PT1	-1.60	23276	5.12	62	1	13		
Sarcalumenin precursor (Srl) 3,4	Q7TQ48	-4.16	54287	6.21	874	17	30		
GrpE protein homolog 1 (Grpel1) 28	Q99LP6	-1.60	21302	6.12	292	7	46	Chaperone	
60 kDa heat shock protein (Hspd1) 29	P63038	>-50	57959	5.30	290	5	12		
Heat shock protein 75 kDa (Trap1) 1	Q9CQN1	8.24	73783	5.73	61	1	1		
Heat shock protein HSP 90-alpha (Hsp90aa1) 1	P07901	8.24	84657	4.93	100	2	3		
Heat-shock protein beta-1 (Hspb1) 26,27	*P14602	2.69 -1.75	23014	6.12	602	12	66		
Protein DJ-1 (Park7) 28	Q99LX0	-1.60	20021	6.32	735	13	91		
T-complex protein 1 subunit beta (Cct2) 4	P80314	-4.73	57346	5.98	1262	25	77		
Caspase-8 precursor (Casp8) 4	O89110	-4.73	55357	5.12	32	1	2	Synthesis/Degradation	
Leukocyte elastase inhibitor A (Serpinb1a) 12	Q9D154	>-50	42575	5.85	47	1	7		
Proteasome subunit alpha type 1 (Psma1) 18	Q9R1P4	30.80	29546	6.00	274	6	37		
Proteasome subunit beta type 7 precursor (Psmb7) 21	P70195	3.90	25252	5.84	388	7	44		
SAPK substrate protein 1 (Ubxn1) 8	Q922Y1	2.25	33572	5.22	41	1	4		
Transcription elongation factor B polypeptide 2 (Tceb2) 30	P62869	>-50	13170	4.87	108	2	30		
Ubiquinone biosynthesis monooxygenase COQ6 (Coq6) 7	Q8R1S0	-5.00	50705	6.55	407	9	35		
Ubiquitin carboxyl-terminal hydrolase isozyme L1 (Uchl1) 25	Q9R0P9	-1.90	24838	5.14	223	5	45		
Chloride intracellular channel protein 4 (Clic4) 20	Q9QYB1	-2.51	28597	5.45	578	12	70	Transport	
Fatty acid-binding protein, heart (Fabp3) 31	P11404	-3.33	14810	6.11	63	1	10		
Frataxin (Fxn) 30	O35943	>-50	18573	5.76	46	1	5		
Tripartite motif-containing protein 72 (Trim72) 2,3,4	Q1XH17	-4.00	52783	6.01	1066	20	75		
Transitional endoplasmic reticulum ATPase (Vcp) 1	Q01853	8.24	89190	5.14	1821	29	48		

Figure 6.

Stem cell therapy-specific subproteome. (**A**): Comparison of stem cell-treated [ES(+)] versus untreated [ES(−)] left ventricular tissue extracts by two-dimensional (2D) electrophoresis. Differentially expressed spots isolated for identification by LTQ-Orbitrap mass spectrometric analysis are circled, and numbered on the ES(+) gel. Inset: Gel-to-gel reproducibility indicated by correlation of scatter plot for average normalized densitometric intensities of matching protein spots from ES(+) versus ES(−) gels. (**B**): Identities of the 61 proteins significantly altered by cell therapy are listed with their symbol (Swiss-Prot gene abbreviation) and spot numbers to locate corresponding 2D gel position(s) in panel (**A**). Mascot score, number of unique identified peptides, % sequence cov. (coverage), predicted

M_r and p*I* for each protein (following expected post-translational processing, for example, removal of a mitochondrial signal peptide), and fold change in ES(+) versus ES(−) are indicated. For proteins detected in more than one spot, maximum score and corresponding number of unique peptides are reported. Fold change was calculated as described in experimental procedures, and for proteins detected in both increasing and decreasing spots (*), both values are indicated. Abbreviations: ES, embryonic stem cells; Ox., oxidative; TCA cycle, tricarboxylic acid cycle; SAPK, stress activated protein kinase.

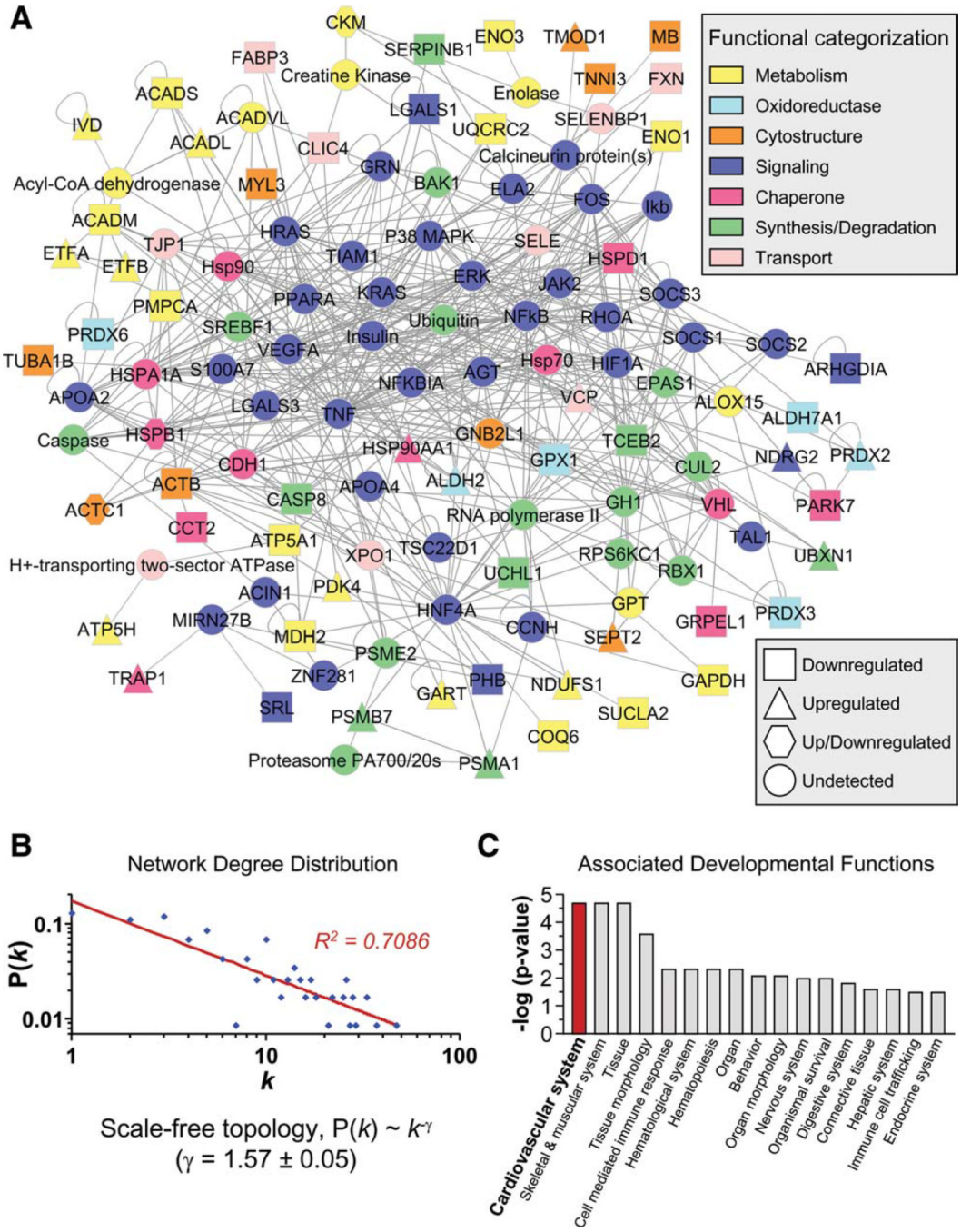

Figure 7.

Cardiovascular system development prioritized in stem cell therapy-specific network. (**A**): Submission to Ingenuity Pathways Analysis (IPA) of differentially expressed proteins in the ES(+)-treated hearts generated a 120-protein interaction network, functionally categorized and color-coded by Swiss-Prot ontological annotation (upper legend), with proteins designated by symbols corresponding to Swiss-Prot gene abbreviations or by family name for nodes representing protein families, and shape indicating directionality of focus protein expression change (lower legend). (**B**): A log-log plot of ES(+)-specific degree distribution [P(*k*)] versus degree (*k*) followed a power law distribution, indicating scale-free, nonstochastic network architecture. (**C**): Bioinformatic interrogation of IPA for associated

developmental functions revealed prioritization of cardiovascular system development in the ES(+)-de-pendent proteome in response to cell therapy. Abbreviations: P(*k*), degree distribution; *k*, node degree.